FINITE TEMPERATURE EFFECTS ON DECAY RATES IN THE REAL-TIME FORMALISM

Two-body decays involving neutral (pseudo)scalars and charged spin-$\frac{1}{2}$ fermions

———————————————

Torbjörn Lundberg
torbjorn.lundberg@thep.lu.se

Department of Astronomy and Theoretical Physics, Lund University

Thesis for a degree of
MASTER OF SCIENCE

supervised by Roman Pasechnik,
co-supervised by Hugo Serôdio

Abstract

This thesis work presents thermal decay rates for several reactions calculated within the framework of the real-time formalism. Processes considered are those of a neutral (pseudo)scalar decaying into two distinct (pseudo)scalars or into a fermion-antifermion pair. These processes are extended from earlier work to include chemical potentials and distinct species in the final state. A hypothetical (pseudo)scalar emission off a fermion line is also presented. The thermal decay rates at high temperature are found to be enhanced relative to zero-temperature theory in the case of (pseudo)scalar-(pseudo)scalar or (pseudo)scalar-fermion final state with quadratic and linear enhancement respectively. A suppression of the (pseudo)scalar decay rate into a fermion-antifermion final state, related to the Pauli principle, is found.

Populärvetenskaplig sammanfattning (Swedish)

Författaren av denna uppsats är partikelfysiker, till på köpet *teoretisk* partikelfysiker. Detta innebär att jag är intresserad av att beskriva och förstå universums absolut minsta beståndsdelar. Den moderna fysiken har, genom hårt arbete av många ytterst kompetenta hjärnor, byggt en modell av det minsta vi känner till: de fundamentala partiklarna. Med exotiska namn som kvarkar, gluoner, fotoner och elektroner utgör denna samling av troligtvis odelbara byggstenar det som vanligen kallas för Standardmodellen. Denna modell har, under lång tid, oerhört framgångsrikt lyckats beskriva nästan allt beteende hos den materia som omger oss i vardagen. Med beteenden menas här alla de sätt som Standardmodellens partiklar kan växelverka (interagera) sinsemellan.

Något som har engagerat en del teoretiska fysiker under det senaste halva århundradet är frågan om de fundamentala partiklarna alltid beter sig likadant. Exempelvis kan man undra om det är givet att beteenden som partikelsönderfall, kollisioner och strålning, som vi känner från det universum som omger oss idag, alltid har varit möjliga. Det är inte otänkbart att sådana processer kan förstärkas eller försvagas utifall en partikels omgivning kraftigt förändras i jämförelse med vårt nuvarande universum.

Som exempel på ett scenario har jag undersökt enkla partikelsönderfall i detta arbete; med sönderfall avses här en situation där en partikel i rörelse splittras till två andra partiklar. Sannolikheten för ett sådant sönderfall kan beräknas med metoder som fysiker har utvecklat under ca. 100 års tid, ett ramverk som kallas för *kvantfältteori*. Jag har undersökt hur sannolikheten för ett sönderfall påverkas när en partikel färdas genom ett oerhört varmt universum. För denna analys har jag använt mig av en vidareutvecklad version av kvantfältteori och har bekräftat att olika sorters partiklar (elektroner respektive Higgspartiklar) båda ändrar sitt beteende när de utsätts för höga temperaturer. Dessa två partiklars beteende ändras dock på helt olika sätt. När Higgspartiklar skapas i sönderfall ökar sannolikheten för hela processen när det blir varmare medan den istället minskar om sönderfallet producerar elektroner (och dess antipartikel). Att sönderfall som skapar elektroner eller Higgspartiklar skiljer sig för höga temperaturer är en fundamental skillnad mellan dessa två partikelsorter och det är därför mycket intressant att studera orsaken till detta fenomen för att förstå naturens fundamentala byggstenar.

Contents

1   Introduction

The ordinary theoretical treatment of fundamental particles primarily uses the language of quantum field theory (QFT), see for example [1–3]. This treatment has historically been extremely successful in describing the behaviour of all the known particles that collectively form the Standard Model of particle physics. However, the theoretical framework of this *zero-temperature theory* does not naturally incorporate effects of the medium relevant for high temperatures and densities. Currently, there is limited understanding of such systems even though several authors have worked on the development of formalisms for treating the medium both in and out of equilibrium. The problem of thermal dynamics has engaged physicists for a long time, and early attempts of analysis were made by for example Bloch [4]. One pioneer in the realm of *thermal quantum field theory* (TFT) was Matsubara [5] who developed the imaginary-time (or Matsubara) formalism that describes equilibrated systems. This treatment has great resemblance to zero-temperature QFT in the form of the propagators and theself-energies. It differs, however, in the treatment of time by taking it to be a purely imaginary quantity. Shortly afterwards, Kubo [6] and Martin and Schwinger [7] provided an important relation between propagators, the so-called Kubo-Martin-Schwinger (KMS) condition, which must hold for thermal propagators at equilibrium. Further important developments of theories with equilibrated media, such as including real times, were made by Keldysh [8]. *Thermo field dynamics*, a first principle analysis, was largely developed by Matsumoto et al. [9] while a detailed investigation of QFTs at finite temperatures was made by Niemi and Semenoff [10].

Comprehensive outlines of the path-integral treatment of quantum fields in a thermal medium may be found in [11, 12], and much of the theoretical basis of this thesis draws upon that work. Just a few years earlier, Weldon [13] provided self-energy calculations using the Matsubara formalism and presented a condensed and clear overview on a quantity interpreted as the *thermal decay rate*.

In order to explain temperature effects in the hot and dense state of the early Universe or in heavy ion collisions in accelerators, a formalism for treating nonequilibrium systems must be in place. It should be mentioned that several authors have worked over the last four to five decades to provide tools for such analysis. Major contributions have come from Danielewicz [14] through general work on QFT at finite temperature, while Wagner [15] provided a detailed outline of nonequilibrium propagators and self-energies in great generality.

This thesis work seeks to provide further emphasis on the importance of thermal theories by means of presenting explicitly the effects of finite temperature on observable thermal decay rates for several decay processes. In the following Sec. 2, a discussion of the underlying theory is presented beginning with the very general formulation of a statistical mechanics principle introduced in QFT by Wagner [15]. This general approach is valid in equilibrium as well as out of equilibrium. Afterwards, the equilibrium propagator is presented, transitioning into an overview of the Matsubara formalism and the real-time formalism. Having the real-time propagators and self-energies established, the concept and definition of the thermal decay rate is presented. In Secs. 3-6, resulting thermal decay rates are presented in the real-time formalism for several processes. This work has been concerned with a (pseudo)scalar particle decaying into two distinct (pseudo)scalars, Sec. 3, a (pseudo)scalar decaying into a fermion-antifermion pair, Secs. 4-5, and finally in Sec. 6, a (pseudo)scalar emission off a fermion line.

The importance of obtaining equilibrium observables should be noted since any nonequilibrium quantity may be matched to a series of master integrals from equilibrium theory [16]. Equilibrium decay rates are specifically needed as input for nonequilibrium calculations.

2 Theoretical background

This section provides the theoretical formulation of TFT and concludeswith an expression for the thermal decay rate. The decay rate of a 1-to-2-transition is related to the self-energy of the eye-diagram. In order to obtain a diagrammatic formulation of TFT, Green's function techniques are deployed in terms of a thermodynamic extension of Wick's theorem.

2.1 Statistical treatment of initial states

The underlying principle of TFT will be outlined in this section. The discussion is mainly based on the broad-ranging and comprehensive article by Wagner [15] and the initial formulas are valid in equilibrium as well as out of equilibrium for arbitrary initial distributions. This general treatment precedes any discussion of equilibrium theories, e.g. the Matsubara formalism or the real-time formalism, and aims to introduce the underlying fundamental statistical principle of TFT as manifested in Eq. (2.2) below.

2.1.1 Operator expectation values

Experimentally measurable observables in QFT are expressed as expectation values of operators evaluated at any given time. An arbitrary experiment is defined by two properties outlined in the following.

The first property to consider is the preparation of the initial state which fully specifies the system at some initial time t_{in}. It is reasonable to assume that no initial state can be determined exactly; rather, one should adopt the view that the initial state can be prepared up to a probability distribution ρ over pure states so that the initial preparation of any system results in a *mixed quantum state*. Mixed states are statistical ensembles of pure states where the ensemble specifies some lack of knowledge of the system e.g. due to noise, entanglement with larger systems, etc. Using the language of statistical quantum mechanics, the distribution ρ assigns a weight $\rho(n) \in [0,1]$ to the pure states $|n\rangle$ where the weights describe the fraction of the ensemble in each state. The weights are normalised according to $\sum_n \rho(n) = 1$ and, in the Fock space spanned by $|n\rangle$, they provide a definition of the *density matrix*:

$$\hat{\rho}(t_{in}) = \sum_n |n(t_{in})\rangle \, \rho(n) \, \langle n(t_{in})| \, . \tag{2.1}$$

This expression describes a classical probability distribution over the pure states. Note that any state, with pure or mixed initial preparation, may be described by this formalism[1]. Using statistical mechanics, the operator expectation value (the observable) is given by

$$\langle \hat{\mathcal{O}}(t_{in})\rangle = \text{tr}\left[\hat{\rho}(t_{in})\hat{\mathcal{O}}(t_{in})\right]$$
$$= \sum_n \langle n(t_{in})|\rho(n)\hat{\mathcal{O}}(t_{in})|n(t_{in})\rangle \tag{2.2}$$

at the initial time t_{in} for an observable $\mathcal{O}$. Hence, the initial preparation of a system is equivalent to the determination of $\hat{\rho}(t_{in})$.

With the initial state now dealt with, the second property to consider is the time evolution of the system. This process is specified by the Hamiltonian $\hat{\mathcal{H}}(t)$, and, in the Heisenberg picture, the system evolves according to the Heisenberg equation of motion:

$$i\frac{d}{dt}\hat{\mathcal{O}}_{\mathcal{H}}(t) = [\hat{\mathcal{O}}_{\mathcal{H}}(t), \hat{\mathcal{H}}(t)] + i\frac{\partial}{\partial t}\hat{\mathcal{O}}_{\mathcal{H}}(t). \tag{2.3}$$

---

[1]A pure state $|\Psi\rangle$ has $\hat{\rho} = |\Psi\rangle\langle\Psi|$ and one may in this case note the idempotency $\hat{\rho}^2 = \hat{\rho}$.

The states are time-independent in this picture and specified fully at t_{in}. A consequence of the above equation of motion is that the time-dependent expectation value, the *one-point function*, is given by

$$\langle \hat{\mathcal{O}}_{\mathcal{H}}(t) \rangle = \sum_n \langle n(t_{\text{in}})|\rho(n)\hat{\mathcal{O}}_{\mathcal{H}}(t)|n(t_{\text{in}})\rangle. \qquad (2.4)$$

The subscript $\mathcal{H}$ will be dropped from now on.

2.1.2 Expansion of the density operator

The initial density operator for an arbitrary experiment may be a many-particle operator. Danielewicz [14] provided the most general proof of Wick's theorem stressing the necessary condition that the expectation value must be taken over a one-particle density operator for the theorem to hold. However, the many-particle density operator may be expressed in terms of one-particle quantities as shown by Wagner [15]. The general outline is presented below.

A general many-particle density operator may always be expressed in exponential form by the introduction of an operator $\hat{\mathcal{B}}$. This is done in complete analogy to the formalism developed by Matsubara [5] so that

$$\hat{\rho}(t_{\text{in}}) = \frac{1}{Z} \exp[-\lambda\hat{\mathcal{B}}(t_{\text{in}})], \qquad Z = \operatorname{tr}\exp[-\lambda\hat{\mathcal{B}}(t_{\text{in}})]. \qquad (2.5)$$

Note that for the grand canonical ensemble $\hat{\mathcal{B}} = \hat{\mathcal{H}} - \mu\hat{\mathcal{N}}$ and $\lambda = \beta$, with μ being the chemical potential, $\hat{\mathcal{N}}$ the number operator, and $\beta = T^{-1}$ (inverse temperature), the formalism of Matsubara is recovered. The deeper motivation for introducing the explicit exponential form above is the desire to develop a theory that describes thermal systems. The exponential expression of $\hat{\rho}$ assumes the form of the Boltzmann distribution which appears in any system that exhibits thermal equilibrium. One may define the one-particle density operator $\hat{\rho}_0$:

$$\hat{\rho}_0 = \frac{1}{Z_0} \exp[-\lambda\hat{B}_0], \qquad Z_0 = \operatorname{tr}\exp[-\lambda\hat{B}_0]. \qquad (2.6)$$

Here, the general one-particle operator $\hat{B}_0$ is extracted from $\hat{\mathcal{B}}$ leaving the residual operator $\hat{B}'$: $\hat{B}' = \hat{\mathcal{B}} - \hat{B}_0$. Since $\hat{B}_0$ is defined analogously to the free one-particle Hamiltonian of zero-temperature theory, a generalised 'interaction picture' can further be defined with respect to the time-independent operator in the Schrödinger picture using $\hat{B}_0$ so that

$$\hat{\mathcal{O}}_{B_0}(\tau) = \exp[i\tau\hat{B}_0]\hat{\mathcal{O}}_S(t_0)\exp[-i\tau\hat{B}_0]. \qquad (2.7)$$

Comparing the translation operators (exponentials) on the right-hand side above to that of Eq. (2.6), one is led to introduce the parameter τ further elaborated on below. Making use of this 'interaction picture' to express the residual of $\hat{\mathcal{B}}$ after the extraction of $\hat{B}_0$, Wagner [15] defined an expansion of the many-particle $\hat{\rho}$ in terms of the one-particle $\hat{\rho}_0$. From Eq. (2.5)

$$\hat{\rho} = \frac{Z_0}{Z}\hat{\rho}_0\hat{S}_{C_\nu}(\tau,0), \qquad \tau = -i\lambda. \qquad (2.8)$$

Here, the parameter τ is purely imaginary for real λ and it defines an imaginary contour of integration C_ν in the complex plane, see Fig. 1. The new operator, an analogue to the time evolution operator of zero-temperature theory, was introduced above as identically being

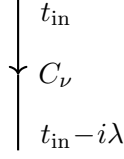$$\hat{S}_{C_\nu}(\tau,0) = \exp[i\tau\hat{B}_0]\exp[-i\tau\hat{\mathcal{B}}]. \qquad (2.9)$$

Figure 1: **The generalised contour of Matsubara.** For the choice of the thermal density operator the end-point is $t_{\text{in}} - i\beta$.

Since $\hat{S}_{C_\nu}(\tau, 0)$ satisfies

$$i\frac{\partial}{\partial \tau}\hat{S}_{C_\nu}(\tau, 0) = \hat{B}'_{B_0}(\tau)\hat{S}_{C_\nu}(\tau, 0), \tag{2.10}$$

the operator may be formally integrated as

$$\hat{S}_{C_\nu}(\tau, 0) = T_{C_\nu}\exp\left[-i\int_0^\tau \mathrm{d}\tau'\, \hat{B}'_{B_0}(\tau')\right] \tag{2.11}$$

by contour-ordering the exponential along the vertical contour segment that goes from 0 to $-i\lambda$ according to

$$T_{C_\nu}\hat{\mathcal{O}}_1(\tau_1)\hat{\mathcal{O}}_2(\tau_2) = \begin{cases} \hat{\mathcal{O}}_1(\tau_1)\hat{\mathcal{O}}_2(\tau_2) & \tau_1 \geq \tau_2 \text{ on } C_\nu, \\ \eta\hat{\mathcal{O}}_2(\tau_2)\hat{\mathcal{O}}_1(\tau_1) & \tau_1 < \tau_2 \text{ on } C_\nu. \end{cases} \tag{2.12}$$

The sign expressed by $\eta = +1\,(-1)$ considers the case of commuting (anticommuting) operators. As mentioned, $\hat{B}'$ has been expressed in the generalised interaction picture with respect to $\hat{B}_0$. Wagner then provides the arbitrary expectation value at t_{in} as

$$\langle\hat{\mathcal{O}}(t_{\text{in}})\rangle = \frac{Z_0}{Z}\sum_{n_0}\langle n_0(t_{\text{in}})|\rho_0\hat{S}_{C_\nu}\hat{\mathcal{O}}(t_{\text{in}})|n_0(t_{\text{in}})\rangle\,. \tag{2.13}$$

This has the same form as Eq. (2.4) if one regards $(Z_0/Z)\hat{S}_{C_\nu}\hat{\mathcal{O}}(t_{\text{in}})$ as the noninteracting (i.e. expressed in the interaction picture) operator to be averaged with respect to $\hat{\rho}_0$. Notably, $\hat{\rho}_0$ is a *one-particle* density operator defined at the initial time t_{in}. As a consequence, Wick's theorem holds for each term in the expansion of $\hat{S}_{C_\nu}$. The emerging contour of integration is the vertical line of Fig. 1. The formalism achieved by the discussion above is valid for any system that is defined by a distribution of the exponential thermal form of Eq. (2.6) at some initial point. Quite generally, the formalism has been shown to hold for a wide family of systems since the many-particle initial distribution may always, at least formally, be expressed in terms of quantities that obey Wick's theorem.

2.1.3 Expansion of the time evolution operator

The time evolution operator, formally defined by Eq. (2.11), evolves the operator to be averaged along the contour of Fig. 1. In this section, its definition will be extended so as to incorporate the real axis and thereby allowing for real temporal arguments.

Wagner [15] states that the time evolution operator must be a one-particle operator in order for Wick's theorem to hold. However, the general time-dependent Hamiltonian contains many-particle interactions. This issue was resolved in the previous section in Eq. (2.13) for the vertical contour in Fig. 1 since the expression provides an expansion in which Wick's theorem holds for each term in $\hat{S}_{C_\nu}$. The thermal *n-point functions* defined by

$$\langle\hat{\mathcal{O}}(t_1, t_2, \ldots, t_n)\rangle = \langle\hat{\mathcal{O}}_1(t_1)\hat{\mathcal{O}}_2(t_2)\cdots\hat{\mathcal{O}}_n(t_n)\rangle \tag{2.14}$$
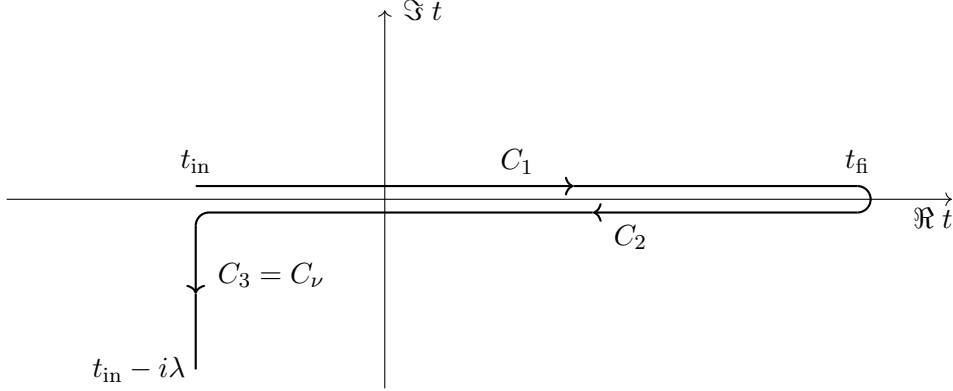
Figure 2: **A partly real-time contour** $C = C_1 \cup C_2 \cup C_3$. The contour is extended along the real axis as to go through the time arguments of any n-point function under consideration. The times t_{in} and t_{fi} are arbitrary and may be suitably chosen for a given system under the condition that all time points of the observable are included. Note that the apparent offset from the real axis is superficial; C_1 and C_2 lie exactly on top of each other and the radii of the arcs connecting the contour segments tend to zero. This figure shows that the real-time contour is a valid choice.

may be extended to include real time-arguments. Keldysh [8] developed an expansion of the time evolution operator. As shown in Fig. 2, a contour segment C_1 that goes up to some largest time t_{fi} on the real axis is added. A second segment C_2 goes back to t_{in}, again along the real axis, before the piece C_3 goes down to $t_{\text{in}} - i\lambda$. The segments on top of the real axis go through all temporal arguments of the n-point function of interest. Note that the apparent offset from the real axis in the figure is purely for display purposes: the two contour pieces C_1 and C_2 lie exactly on top of the axis.

Contour ordering T_C may be defined along this extended contour. In complete analogue to the previous section, the notion of $\hat{\mathcal{B}}$ may be extended by the introduction of

$$\hat{\mathcal{K}}(\tau) = \begin{cases} \hat{\mathcal{H}}(\tau) & \tau \text{ on } C_1 \cup C_2, \\ \hat{\mathcal{B}}(\tau) & \tau \text{ on } C_\nu. \end{cases} \tag{2.15}$$

The procedure may be followed through by the definition of one-particle and residual operators $\hat{K}'$ and $\hat{K}_0$ that are defined over the entire real-time contour, similar to $\hat{\mathcal{K}}$ (see the analogous definition of $\hat{B}'$, $\hat{B}_0$ following Eq. (2.6)). The two-point function may be written as

$$\langle \hat{\mathcal{O}}(t, t') \rangle = \frac{Z_0}{Z} {}_0\langle T_C \hat{S}_C \hat{O}_{K_0}(t, t') \rangle_0 \,. \tag{2.16}$$

The subscripts of the brackets indicate that the trace is to be taken with respect to the one-particle density operator $\hat{\rho}_0$ defined in terms of $\hat{K}_0$. T_C orders operators along the entire contour C and the time evolution operator

$$\hat{S}_C = T_C \exp\left[-i \int_C d\tau \, \hat{K}'_{K_0}(\tau)\right] \tag{2.17}$$

is expressed in the generalised interaction picture analogously to Sec. 2.1.2. Hence, a formulation of an arbitrary system out of equilibrium exists in terms of the series expansion of $\hat{S}_C$

that expresses nonequilibrium quantities in terms of equilibrium ones. Further, the equilibrium quantities are expanded in terms of one-particle functions later in this work in order to obtain a diagrammatic series that describes the observables of interest. For such series, the thermodynamic version of Wick's theorem holds [14].

2.2 The contour path-integral formulation

Specialising to the case of density operators that describe systems in equilibrium, this section outlines the path-integral formulation of thermal systems starting from the grand canonical ensemble, extracts the general propagator of thermal theory and finally defines thermal decay rates. One-particle quantities will be assumed initially and much of the theory is introduced for free particles. Interactions are thereafter introduced perturbatively. The material presented is primarily based on the report by Landsman and van Weert [12] that discusses different formalisms of TFT.

2.2.1 Grand canonical ensemble

In equilibrium, the Hamiltonian $\hat{\mathcal{H}}$ is time-independent, and a system of charged particles is characterised by the density operator of the grand canonical ensemble

$$\hat{\rho} = \exp[-\Phi - \sum_a \alpha_a \hat{Q}_a - \beta \hat{\mathcal{H}}], \qquad \Phi = \log \mathrm{tr} \Big[-\sum_a \alpha_a \hat{Q}_a - \beta \hat{\mathcal{H}} \Big]. \qquad (2.18)$$

Here, $\hat{Q}_a$ are the conserved charges with $a \in \{1, A\}$ and Φ is the thermodynamical potential related to the partition function through $\Phi = -\log Z$. The charge operators $\hat{Q}_a$ and the Lagrange multipliers α_a may be related to the number density operator and the chemical potential respectively as

$$\hat{N}_a = \frac{1}{V} \langle \hat{Q}_a \rangle, \qquad \alpha_a = -\beta \mu_a, \qquad (2.19)$$

where V is the volume of the system and μ_a expresses the chemical potential related to each type of charge. As seen in the previous section, the form of $\hat{\rho}$ determines the expectation value of any n-point function.[2]

2.2.2 The generating functional

Analogous to zero-temperature QFT, n-point correlation functions (thermal Green's functions) of arbitrary field operators $\hat{\Phi}$ can be defined as

$$G_C(x_1, x_2, \dots, x_n) = \langle T_C \hat{\Phi}(x_1) \hat{\Phi}(x_2) \cdots \hat{\Phi}(x_n) \rangle. \qquad (2.20)$$

So far, the contour C may be chosen quite arbitrary but it becomes restricted for diagrammatic formalisms that require the thermodynamic version of Wick's theorem to hold.

The thermal Green's functions can be generated by the functional

$$Z[j] = Z[0] \left\langle T_C \exp\left[i \int_C \mathrm{d}^4 x \, j(x) \hat{\Phi}(x) \right] \right\rangle \qquad (2.21)$$

---

[2]This work presents formalisms and results in the rest frame of the medium for simplicity. A Lorentz-covariant formulation of the grand canonical ensemble has been introduced by Niemi and Semenoff [10].

expressed in terms of the c-number sources $j(x)$ through functional differentiation:

$$G_C(x_1, x_2, \ldots, x_n) = \frac{1}{Z[0]} \frac{\delta^n Z[j]}{i\delta j(x_1) \cdots i\delta j(x_n)} \bigg|_{j=0}. \tag{2.22}$$

The normalisation is $Z[0] = \exp[\Phi(\beta, V)]$.

Time ordering on the contour, T_C, may be explicitly expressed by parametrising C according to $t = z(\tau)$ with τ being real and monotonically increasing along the contour. Through the definition of the *contour step function*

$$\Theta_C(t - t') = \Theta(\tau - \tau'), \tag{2.23}$$

the two-point function, taken as an example, is

$$G_C(x, x') = \Theta_C(t - t') \langle \hat{\Phi}(x) \hat{\Phi}(x') \rangle + \eta \Theta_C(t' - t) \langle \hat{\Phi}(x') \hat{\Phi}(x) \rangle. \tag{2.24}$$

$\eta = \pm 1$ for commuting/anticommuting (bosonic/fermionic) field operators. Weldon [13] showed that this expression is well behaved only if the imaginary component of the contour C never increases with τ. Feynman, Matthews and Salam [2,3] provided the first proof of this statement in the context of the path-integral formulation.

It should be mentioned at this point that the terms *scalar*, *boson* and *fermion* will be used extensively throughout the following theoretical outline, as well as *commuting* and *anticommuting* fields and operators. Some of those labels are used slightly different by different authors and this paragraph shall shed some light on how the terms are used within this work. The term 'scalar' intends to reference a scalar quantity both in Lorentz and in any internal space. Hence, a 'scalar field' associates a single value to each point in space-time but *it may be either a commuting or an anticommuting field (the latter being a Grassmann variable)* in this thesis. A 'boson' refers to an operator that obeys canonical *commutation* relations. Hence, a 'scalar boson' is the specification of a scalar (i.e. not a vector) field that obeys Bose-Einstein statistics. The use of the term 'fermionic scalar' in this thesis might induce some confusion for the reader; the label refers to a scalar (i.e. not a vector) field that anticommutes. This distinction of scalars is introduced simply because it is an easier exercise and a common approach in literature to present the initial theory in terms of either commuting or anticommuting scalar fields. The formalism is then later extended to include fields that carry Lorentz or spin components. Hence, proper care must be taken when constructing a Lagrangian so as to only include field types with the proper structure in Lorentz and spin space respecting the conservations laws of the universe. The term 'fermion' is applied along its most common usage to Dirac spinors that carry components in spin space.

Note, however, in the result sections 3-6, the theoretical framework has been laid out and the mentioned scalars are assumed to be bosonic in nature for all computed self-energies and decay rates.

2.2.3 The path-integral formulation

The functional that generates n-point functions was stated in the previous section as a thermal expectation value. In the path-integral formulation, the state vectors that span the Fock space of Sec. 2.1 may be substituted for a basis of *coherent states* that expresses the state of the

quantum fields in terms of the continuous three-space variable $\mathbf{x}$. In such basis, the states are $|\phi(\mathbf{x}); 0\rangle$ at time $t = 0$ and are eigenstates of the field operator $\hat{\phi}(x)$:

$$\hat{\phi}(x)\,|\phi(\mathbf{x}); 0\rangle = \phi(x)\,|\phi(\mathbf{x}); 0\rangle\,, \qquad \hat{\phi}(x) = e^{i\hat{H}t}\hat{\phi}(0, \mathbf{x})e^{-i\hat{H}t}. \tag{2.25}$$

The *neutral bosonic* field considered in this section provides a simple example with vanishing chemical potential. The thermal trace in the generating functional for such field explicitly becomes

$$Z[j] = \int [\mathcal{D}\varphi]\,\langle \varphi; t_{\mathrm{in}}|e^{-\beta\hat{H}}T_C \exp\!\left[i\int_C \mathrm{d}^4x\,j(x)\hat{\phi}(x)\right]|\varphi; t_{\mathrm{in}}\rangle\,. \tag{2.26}$$

Given the time evolution of the field operator in Eq. (2.25), the following time evolution must be induced:

$$|\phi(\mathbf{x}); t\rangle = e^{i\hat{H}t}\,|\phi(\mathbf{x}); 0\rangle\,. \tag{2.27}$$

The action of the canonical density operator in the right-hand side trace of Eq. (2.26) can then analogously be interpreted as a complex shift in time:

$$\langle \varphi; t_{\mathrm{in}}|\,e^{-\beta\hat{H}} = \langle \varphi; t_{\mathrm{in}}\!-\!i\beta|\,. \tag{2.28}$$

This, so far, purely formal equivalence of the thermal density operator to the time-evolution operator was first noted by Bloch [4] already in 1932 and from this observation follows the introduction of the complex temporal contour of Sec. 2.1. Note specifically that the eigenvalue of the field operator remains in order for the trace interpretation to hold. Hence, the functional measure $[\mathcal{D}\varphi]$ may only pick out fields with this periodicity condition over $i\beta$ so that $\varphi(t_{\mathrm{in}}, \mathbf{x}) = \varphi(t_{\mathrm{in}} - i\beta, \mathbf{x})$. With the formal observation above, the shifted trace can be restated in terms of some arbitrary initial and final times t_{i}, t_{f} with the aid of the Feynman-Salam-Matthews (FSM) formula [2, 3]:

$$\langle \varphi_{\mathrm{f}}(\mathbf{x}); t_{\mathrm{f}}|T_C F[\hat{\phi}]|\varphi_{\mathrm{i}}(\mathbf{x}); t_{\mathrm{i}}\rangle = \mathcal{N}' \int [\mathcal{D}\phi]\,F[\phi]e^{iS[\phi]} \tag{2.29}$$

if the path-integral on the right-hand side is taken over all c-number fields that satisfy the boundary conditions

$$\phi(t_{\mathrm{i}}, \mathbf{x}) = \varphi_{\mathrm{i}}(\mathbf{x}) \quad \text{and} \quad \phi(t_{\mathrm{f}}, \mathbf{x}) = \varphi_{\mathrm{f}}(\mathbf{x}). \tag{2.30}$$

Eq. (2.29) remains valid for arbitrary initial and final times under the single restriction that the imaginary component of the integration contour C connecting t_{i} and t_{f} may not increase along the direction of the contour [12]. Hence, C must go downwards in the complex plane or extend in parallel to the real axis. The normalisation $\mathcal{N}'$ may absorb a Gaussian integration over the conjugate momentum in $S[\phi]$ so that $\mathcal{N}' \to \mathcal{N}$ below. The action is then

$$S[\phi] = \int_{t_{\mathrm{i}}}^{t_{\mathrm{f}}} \mathrm{d}t \int \mathrm{d}^3x\,\mathcal{L}(x) \underset{\substack{\text{For } t_{\mathrm{i}}, t_{\mathrm{f}} \\ \text{connected} \\ \text{by } C.}}{\longrightarrow} \int_C \mathrm{d}^4x\,\mathcal{L}(x), \tag{2.31}$$

and hence the generating functional becomes

$$\begin{aligned}
Z[j] &= \mathcal{N} \int [\mathcal{D}\phi]\,\exp\!\left[i\int_C \mathrm{d}^4x\,\big(\mathcal{L}(x) + j(x)\phi(x)\big)\right] \\
&= Z[0]\left\langle \exp\!\left[i\int_C \mathrm{d}^4x\,j(x)\phi(x)\right]\right\rangle.
\end{aligned} \tag{2.32}$$

Here, $t_i = t_{in}$ and $t_f = t_{in} - i\beta$ are connected through C. Expressed as a path-integral in terms of fields rather than operators, the generating functional has absorbed the contour time ordering. The statistical average has been reinterpreted in the path-integral formulation to be taken with respect to the action. The ill-defined[3] normalisation $Z[0]$ cancels out in the thermal Green's functions of Eq. (2.22).

2.2.4 Propagator of the free neutral scalar boson

In the special case of a free particle with no derivative couplings[4], here a neutral boson with the free Lagrangian

$$\mathcal{L}_0(x) = \tfrac{1}{2}\phi(x)\bigl(-\partial^2 - m^2\bigr)\phi(x), \tag{2.33}$$

the *free* generating functional may be rewritten from Eq. (2.32) by means of a change of variables:

$$Z_0[j] = Z_0[0]\exp\left[-\frac{i}{2}\int_C \mathrm{d}^4x \int_C \mathrm{d}^4x'\, j(x)D_C(x-x')j(x')\right]. \tag{2.34}$$

$$\text{Here} \quad \phi(x) \to \phi(x) - \int_C \mathrm{d}^4x'\, D_C(x-x')j(x'). \tag{2.35}$$

The shift of $\phi(x)$ is chosen carefully in order to complete the square of the free Lagrangian. The emerging *thermal bosonic propagator* $D_C(x-x')$ is defined in relation to the differential operator of the equation of motion and satisfies

$$K(i\partial)D_C(x-x') = \delta_C(x-x') \qquad \text{for} \qquad K(i\partial)\phi(x) = 0. \tag{2.36}$$

For the neutral boson $K(i\partial)\phi(x) = -(\partial^2 + m^2)\phi(x) = 0$; this is the Klein-Gordon equation. The contour δ-function may be defined as $\delta_C(t - t') = \left(\frac{\partial z}{\partial \tau}\right)^{-1}\delta(\tau - \tau')$ with τ parametrising the contour C (recall the definition $t = z(\tau)$). The propagator is therefore related to the free two-point function (Green's function)

$$G_{0C}(x,x') \equiv iD_C(x-x'). \tag{2.37}$$

The propagator can be written in the *spectral representation*:

$$iD_C(x-x') = \int \frac{\mathrm{d}^4k}{(2\pi)^4}\, \rho_0(k)e^{-ik\cdot(x-x')}\bigl[\Theta_C(t-t') + n(k_0)\bigr], \qquad \eta = +1. \tag{2.38}$$

This result was first derived by Mills according to Landsman and van Weert [12], and, for normal time ordering, this is the expression presented by Dolan and Jackiw [17]. The *spectral density* for the free neutral bosonic field is

$$\rho_0(k) = 2\pi\,\text{sign}(k_0)\delta\bigl(k^2 - m^2\bigr). \tag{2.39}$$

---

[3]The measure $[\mathcal{D}\phi]$ denotes all sufficiently differentiable and integrable functions that must be taken into account when considering all paths. However, the total number of functions is vastly larger and there exists no rigorous method of picking out only the physically relevant functions in the path-integral. If the reader, nevertheless, is familiar with the path-integral formulation, one simply ignores this lack of rigour and presses on.

[4]No such couplings are assumed to exist in the theory in order for the integration of the canonical momentum variable in the generating functional to be performed. A consequence is that the free scalar action $S = \int \mathrm{d}^4x\,\tfrac{1}{2}\bigl(\partial_\mu\phi\partial^\mu\phi - m^2\phi^2\bigr) \to \partial_\mu\left(\int \mathrm{d}^4x\,\tfrac{1}{2}\phi\partial^\mu\phi\right) + \int \mathrm{d}^4x\,\tfrac{1}{2}\phi\bigl(-\partial^2 - m^2\bigr)\phi.$

Note that this quantity is not related to the distribution in Sec. 2.1 and the latter ρ will not appear from this point on other than in its explicit exponential form. The *thermal distribution function* $n(k_0)$ may be derived from the expectation value of pairs of creation/annihilation operators and for equilibrium dynamics, it is the Bose-Einstein/Fermi-Dirac distribution for bosonic/fermionic fields:

$$n(k_0) = \frac{1}{e^{\beta k_0} - \eta}. \tag{2.40}$$

This distribution guarantees that the fields satisfy the periodicity condition imposed by the trace interpretation. Quite often, the propagator in Fourier space is used and transformation of the expression for D_C above gives[5]

$$i\tilde{D}(k) = i\int \frac{\mathrm{d}k_0'}{2\pi} \frac{\rho_0(k_0', \mathbf{k})}{k_0 - k_0' + i\epsilon} + \rho_0(k)n(k_0). \tag{2.41}$$

The thermal propagator has thus been split into a leading part that resembles the expression from zero-temperature theory and an additional thermal term which vanishes in the limit $T \to 0$. Using the spectral density of Eq. (2.39), the integral may be performed and the first term of this transformed propagator can be rewritten in terms of the Feynman propagator of zero-temperature theory. The result can be seen for example in Eq. (2.95) using Eqs. (2.93)-(2.94).

Splitting the Lagrangian into its free and interaction parts as $\mathcal{L} = \mathcal{L}_0 + \mathcal{L}_\mathrm{I}$, the free Lagrangian may be used to factor out the free generating functional of Eq. (2.34) from the full generating functional of Eq. (2.32). To obtain Feynman rules and a diagrammatic series, the full $Z[j]$ is rewritten analogous to zero-temperature theory as

$$Z[j] = \exp\left[i\int_C \mathrm{d}^4x \, \mathcal{L}_\mathrm{I}\left[\frac{\delta}{i\delta j(x)}\right]\right] Z_0[j]. \tag{2.42}$$

This expression is swiftly derived through a series expansion of $\exp\left[i\int_C \mathrm{d}^4 \, \mathcal{L}_\mathrm{I}(x)\right]$. By observing that the series can be obtained by functional differentiation w.r.t. the source $j(x)$, the argument of $\mathcal{L}_\mathrm{I}$ may be replaced by the functional differential, and the exponentiated interaction term can be taken out of the functional integral.

The generating functional of Eq. (2.42) contains all n-point functions $G_C(x_1, \ldots, x_n)$. Analogous to zero-temperature theory, all *disconnected diagrams* can be factorised out by considering only the *connected Green's functions* $G_C^{(n)}(x_1, \ldots, x_n)$ defined by

$$G_C^{(n)}(x_1, \ldots, x_n) = \left.\frac{\delta^n W[j]}{i\delta j(x_1) \cdots i\delta j(x_n)}\right|_{j=0}, \qquad W[j] = \log Z[j]. \tag{2.43}$$

The expansion of $W[j]$ is often referred to as the *cumulative expansion* and the resulting series trivially generates the connected Green's functions, i.e. the sum of all diagrams that are fully connected.

$$W[j] = \log Z[0] + \sum_{n=1}^{\infty} \frac{i^n}{n!} \int \cdots \int \mathrm{d}^4x_1 \cdots \mathrm{d}^4x_n \, G_C^{(n)}(x_1, \ldots, x_n) \cdot j(x_1) \cdot \ldots \cdot j(x_n). \tag{2.44}$$

As a consequence of the log-relation of $Z[j]$ to $W[j]$, the contribution from all disconnected diagrams factorises and may be absorbed by the normalisation of the Green's functions.

---

[5] Use $\Theta(x_0) = \frac{i}{2\pi}\int_{-\infty}^{+\infty}\mathrm{d}\tau \frac{1}{\tau + i\epsilon}e^{-ix_0\tau}$ in the limit $\epsilon \to 0^+$ in the transform.

2.3 Thermal propagators

In the previous section, the propagator of a free neutral boson was related to the two-point function. The latter will be of great importance for this thesis work and it is given by the evaluation of expectation values in the form

$$\langle \hat{\mathcal{O}}(t,t') \rangle = \langle \hat{\mathcal{O}}_1(t)\hat{\mathcal{O}}_2(t') \rangle \tag{2.45}$$

while making use of the contour time ordering procedure, see Sec. 2.2.2. This section can be seen as a generalisation of Sec. 2.2.4 and follows closely Landsman and van Weert [12].

2.3.1 The general generating functional

Consider a general multi-component covariant complex field (bosonic or fermionic) described by the operator $\hat{\mathbb{\Phi}}^i_\alpha(x)$ [12]. Here, α is the index of the Lorentz representation of the field, e.g. a spinor or vector index and i is an index of a representation of an internal symmetry or a field generation index, i.e. not related to space-time transformations. Let the operator transform under some representation of the Lorentz group $\mathcal{J}_{\alpha\beta}[\Lambda]$. The field will be charged under any internal symmetries and the conserved charges are denoted as q^{ij}_a so that

$$\left[\hat{Q}_a, \hat{\mathbb{\Phi}}^i_\alpha(x)\right] = -q^{ij}_a \hat{\mathbb{\Phi}}^j_\alpha(x). \tag{2.46}$$

The chemical potential for fields charged under multiple symmetries is generally given by $\mu = \sum_a \mu_a q_a$, (see the grand canonical ensemble in subsection 2.2.1 applied to eigenstates of $\hat{Q}_a$: $\sum_a \mu_a \hat{Q}_a |\mathbb{\Phi}\rangle = \sum_a \mu_a q_a |\mathbb{\Phi}\rangle$). A theory with no derivative couplings may be assumed to have a free Lagrangian of the quadratic form

$$\mathcal{L}_0(x) = \bar{\mathbb{\Phi}}^i_\alpha(x) K^{ij}_{\alpha\beta}(i\partial, \mu)\mathbb{\Phi}^j_\beta(x). \tag{2.47}$$

The *adjoint field* is defined as $\bar{\mathbb{\Phi}}^i_\alpha = (\mathbb{\Phi}^\dagger \mathcal{A})^i_\alpha$.[6] $K^{ij}_{\alpha\beta}(i\partial, \mu)$ is the differential operator of the free field in the medium which generally depends on the chemical potential. The free thermal Green's functions that arise from this Lagrangian can be obtained from the generating functional. In the path-integral formulation, this functional may be written in terms of two source fields:

$$Z_0[\bar{\jmath}, j] = \mathcal{N} \int [\mathcal{D}\bar{\mathbb{\Phi}}] \int [\mathcal{D}\mathbb{\Phi}] \exp\left[i\int_C \mathrm{d}^4x \left(\bar{\mathbb{\Phi}}K\mathbb{\Phi} + e^{i\mu t}\bar{\jmath}\mathbb{\Phi} + e^{-i\mu t}\bar{\mathbb{\Phi}}j\right)\right]. \tag{2.48}$$

$j(x)$ is the source of $\mathbb{\Phi}$ while $\bar{\jmath}(x)$ is the source of $\bar{\mathbb{\Phi}}$. The μ-dependence has been shifted away from K to the source terms by means of a change of variables introduced by Weldon [18] where the fields and the differential operator are transformed as

$$\mathbb{\Phi} \to e^{i\mu t}\mathbb{\Phi}, \qquad \bar{\mathbb{\Phi}} \to e^{-i\mu t}\bar{\mathbb{\Phi}}, \qquad K(i\partial, \mu) \to K(i\partial), \tag{2.49}$$

thus treating the field and its adjoint as independent variables. In this generating functional, the fields are contracted over all discrete indices: $\bar{\jmath}\mathbb{\Phi} = \bar{\jmath}^i_\alpha(x)\mathbb{\Phi}^i_\alpha(x)$.[7]

---

[6]The matrix $\mathcal{A}_{\alpha\beta}$ ensures invariance of the Lagrangian under Lorentz transformations of $\mathbb{\Phi}$. In the case when α is an index of the Dirac spinor representation, $\mathcal{A} = \gamma^0$.

[7]The generating functional of Eq. (2.48) was initially formulated in terms of the $\mathcal{H}$amiltonian density rather than the Lagrangian ditto. The path integral then involves the functional measure over the fields of interest, the adjoint fields, *and* the respective conjugate momenta π_α, $\bar{\pi}_\alpha$. Theories with no derivative couplings fulfil $\pi_\alpha = \dot{\mathbb{\Phi}}_\alpha$, and the Gaussian integral over π_α may be fully absorbed into $\mathcal{N}$.

2.3.2   The general thermal propagator and the KMS condition

The functional integral of Eq. (2.48) is defined in order to generate the thermal Green's functions (n-point functions) under functional differentiation and therefore it must represent the thermal trace of Eq. (2.4):

$$\mathrm{tr}\left[e^{-\beta(\hat{H}-\mu\hat{Q})}T_C\exp\left[i\int_C\mathrm{d}^4x\left(\bar{\jmath}\Phi+\bar{\Phi}j\right)\right]\right].\tag{2.50}$$

In order to recover the trace interpretation of the generating functional, the functional measure is to be taken only over c-number fields Φ, $\bar{\Phi}$ such that the following periodicity condition is satisfied over a period $i\beta$[8]:

$$\Phi_\alpha^i(t_{\mathrm{in}}-i\beta,\mathbf{x})=\eta e^{\beta\mu}\Phi_\alpha^i(t_{\mathrm{in}},\mathbf{x}).\tag{2.51}$$

The periodicity leads to the *Kubo-Martin-Schwinger condition* (KMS) on the propagator which was introduced by Kubo [6], implemented by Martin and Schwinger [7] and is presented in the following.

   The free generating functional of Eq. (2.48) can be rewritten in terms of the *general free thermal propagator* by a shift of the field and its adjoint analogously to the case of the scalar field in Sec. 2.2.4. Contracted over all indices, the result is

$$Z_0[\bar{\jmath},j]=Z_0[0,0]\exp\left[-i\int_C\mathrm{d}^4x\int_C\mathrm{d}^4x'\,\bar{\jmath}_\alpha^i(x)D_{C\,\alpha\beta}^{\,ij}(x-x')j_\beta^j(x')\right]\tag{2.52}$$

with

$$Z_0[0,0]=\mathcal{N}\int[\mathcal{D}\bar{\Phi}]\int[\mathcal{D}\Phi]\exp\left[i\int_C\mathrm{d}^4x\,\bar{\Phi}K\Phi\right].\tag{2.53}$$

In order to complete the square and extract the propagator $D_{C\,\alpha\beta}^{\,ij}\equiv\left(K^{-1}\right)_{\alpha\beta}^{ij}$, the thermal propagator must satisfy the differential equation

$$K_{\alpha\beta}^{ij}(i\partial)D_{C\,\beta\gamma}^{\,jk}(x-x')=\delta_{\alpha\gamma}\delta^{ik}\delta_C(x-x').\tag{2.54}$$

The generating functional must be invariant under the introduced shifts of the fields. This condition fixes the solution of the differential equation so that the propagator can be related to the two-point function as

$$\begin{aligned}iD_{C\,\alpha\beta}^{\,ij}(x-x')&\equiv G_{0C\,\alpha\beta}^{\quad ij}(x,x')\\&=\,_0\langle T_C\hat{\Phi}_\alpha^i(x)\hat{\bar{\Phi}}_\beta^j(x')\rangle_0=\,\langle\Phi_\alpha^i(x)\bar{\Phi}_\beta^j(x')\rangle\,.\end{aligned}\tag{2.55}$$

This is a special case of the general relation Eq. (2.16) with the final expectation value expressed in the path-integral formalism over fields rather than operators, analogously to Eq. (2.32). Guided by the definition of the time ordering T_C, the free propagator may be split using the contour step-function of Eq. (2.23) so that

$$D_{C\,\alpha\beta}^{\,ij}(x-x')=\Theta_C(t-t')D_{\;\;\alpha\beta}^{>\,ij}(t-t')+\Theta_C(t'-t)D_{\;\;\alpha\beta}^{<\,ij}(t-t').\tag{2.56}$$

Compare this to Eq. (2.24) for the general n-point function. The imposed boundary condition on the field of Eq. (2.51) forces a boundary condition on the propagator that relates the

---

[8]Without this condition, the functional integral no longer generates the trace: $\langle\Phi-i\beta|\,\hat{\mathcal{O}}\,|\Phi\rangle\equiv\langle\Phi|\,\hat{\mathcal{O}}\,|\Phi\rangle$.

advanced and retarded components of the time-ordered propagator above. As a consequence, invariance of the path-integral over $i\beta$ holds. This is the KMS-condition:

$$D^{>\,ij}_{\alpha\beta}(t_{\text{in}} - i\beta) = \eta e^{-\beta\mu} D^{<\,ij}_{\alpha\beta}(t_{\text{in}}). \tag{2.57}$$

The condition is important for thermal theories and it relates several thermal quantities in the *real-time formalism*, Sec. 2.5, thereby reducing the number of degrees of freedom.

Note that any relativistic, multi-component field $\Phi^i_\alpha(x)$ should satisfy the Klein-Gordon equation. Therefore, a multi-mass *Klein-Gordon divisor* $d^{ij}_{\alpha\beta}(i\partial)$ exists so that

$$d^{ij}_{\alpha\beta}(i\partial)K^{jk}_{\beta\gamma}(i\partial) = K^{ij}_{\alpha\beta}(i\partial)d^{jk}_{\beta\gamma}(i\partial) = \delta_{\alpha\gamma}\delta^{ik}\prod_l\left(-\partial^2 - m_l^2\right). \tag{2.58}$$

The m_l's represent the mass spectrum and can be inferred from the spin-structure of K [19,20]. For an extended and comprehensive discussion regarding the mass spectrum, see the lecture notes of Wightman [19]. The solution to Eq. (2.54) simply becomes

$$D_C{}^{ij}_{\alpha\beta}(x - x') = d^{ij}_{\alpha\beta}(i\partial_x)D_C(x - x') \tag{2.59}$$

in terms of the scalar propagator encountered earlier. A slight reservation should be made regarding the form of $D_C(x - x')$. The solution presented in Eq. (2.38) of Sec. 2.2.4 is that of a *neutral* scalar boson. When incorporating anticommuting as well as charged fields ($\mu \neq 0$) this propagator is modified slightly to become

$$iD_C(x - x') = \int \frac{\mathrm{d}^4k}{(2\pi)^4}\,\rho_0(k)e^{-ik\cdot(x-x')}\big[\Theta_C(t - t') + \eta n(\omega_+)\big] \tag{2.60}$$

with the distribution function

$$n(\omega_\pm) = \frac{1}{e^{\omega_\pm} - \eta}. \tag{2.61}$$

The $\pm$ denotes charged particles/antiparticles through the definition $\omega_\pm = \beta(k_0 \mp \mu)$. Generally, the spectral density of the free field can be found as

$$\rho_0(k) = i\,\mathrm{Disc}\prod_l \frac{1}{k^2 - m_l^2}. \tag{2.62}$$

The discontinuity is defined over the real axis as $\mathrm{Disc}\,f(k_0) = f(k_0 + i\epsilon) - f(k_0 - i\epsilon)$ with $\epsilon \to 0^+$. The results of this section rely on the fact that the contour step-function commutes with the Klein-Gordon divisor. Further, the charge operators are assumed to commute with $\mathcal{L}_0$ so that the matrices q_a commute with both $K(i\partial)$ and $d(i\partial)$ [12]. The most important points from the above discussion should be stressed as clearly as possible:

- Time integration is to be taken along a contour C that begins at an arbitrary initial time t_{in} and goes down to the final time $t_{\text{in}} - i\beta$ with the restriction that the imaginary component of the contour can not increase.[9]

- The propagator $D_C(x - x')$ depends explicitly on the choice of contour.

---

[9]Recall that the contour is a consequence of the trace interpretation of the path-integral formulation with one of the states shifted by the thermal density operator. The imposed restriction on the imaginary part of the contour is required for the application of the FSM-formula of Eq. (2.29).

These points are valid for all thermal propagators as a consequence of the very general expression of Eq. (2.59). Since the quantities used when performing calculations depend explicitly on the choice of the contour C, it is imperative to choose a formalism where real-time quantities easily can be extracted and more so in a way that the final result does not depend on this choice of C. Two commonly used formalisms will be presented in the following.

2.4 The imaginary-time formalism

The presented thermal formulation of quantum field theory in the sections above formally resembles to a high degree the well-known quantum field theory at zero-temperature. The main distinguishing property is that the explicit form of the thermal n-point function (Green's function) depends on the choice of integration contour C in the complex temporal plane. This contour connects some arbitrary initial time t_{in} with the final time $t_{\mathrm{in}} - i\beta$. This specific final time point emerges as a consequence of the formal interpretation of the thermal equilibrium distribution operator as an evolution operator. To a large extent, the contour that connects the initial and final time points can be arbitrarily chosen in equilibrium theory with the single restriction that the imaginary component of the contour must not increase when integrating along the contour. In this section, a specific choice of contour will be considered in order to perform explicit calculations. The discussion will be followed by a diagrammatic expansion of the generating functional in order to derive the Feynman rules on this contour.

2.4.1 The Matsubara contour

The simplest possible choice of integration contour is due to Matsubara [5]. It constitutes a straight vertical line that connects t_{in} and $t_{\mathrm{in}} - i\beta$, cf. Fig. 1 with $\lambda = \beta$. The time variable may then be parametrised in a simple and purely imaginary way: $t = i\tau$ with $\tau \in [0, \beta]$ being a real variable. This particular choice has the advantage that it generates a perturbative expansion that contains diagrams recognised from zero-temperature theory. This section will mainly be concerned with a single scalar field as a simple example, but the results may be generalised [12] to fields with both Lorentz components and internal symmetries. Through the parametrisation of t, the action may be written as an integral in *Euclidean* space:

$$-S_{\mathrm{E}} = i \int_C \mathrm{d}^4 x \, \mathcal{L}(x) = -\int_0^\beta \mathrm{d}\tau \int \mathrm{d}^3 x \, \mathcal{L}_{\mathrm{E}}(x) \tag{2.63}$$

where the Euclidean Lagrangian is

$$\begin{aligned}
\mathcal{L}_{\mathrm{E}}(\tau, \mathbf{x}) &= \tfrac{1}{2}\phi(\tau, \mathbf{x})\big(-\partial_\tau^2 - \nabla_{\mathbf{x}}^2 + m^2\big)\phi(\tau, \mathbf{x}) + \mathcal{V}(x) \\
&= \tfrac{1}{2}\phi(\tau, \mathbf{x}) K_{\mathrm{E}} \, \phi(\tau, \mathbf{x}) + \mathcal{V}(x).
\end{aligned} \tag{2.64}$$

The n-point Green's functions may be obtained by functional differentiation w.r.t. a source $j(\tau, \mathbf{x})$ of the generating functional

$$Z[j] = \int [\mathcal{D}\phi]\, e^{-S_{\mathrm{E}} + j \cdot \phi}, \qquad j \cdot \phi = \int_0^\beta \mathrm{d}\tau \int \mathrm{d}^3 x \, j(\tau, \mathbf{x})\phi(\tau, \mathbf{x}). \tag{2.65}$$

2.4.2 The imaginary-time propagator

As stated in Eq. (2.34), the free generating functional $Z_0[j]$ (with $\mathcal{V}(x) = 0$) may be written in terms of the free propagator by completion of the square. In the Matsubara formalism, the

result is

$$Z_0[j] = Z_0[0] \exp\left[\tfrac{1}{2} j \cdot K_{\mathrm{E}}^{-1} \cdot j\right]. \tag{2.66}$$

The inverse of the differential operator must satisfy the boundary condition of Eq. (2.36) in order to fix the solution of the differential equation. The solution is the *thermal propagator of Matsubara* $K_{\mathrm{E}}^{-1} = \Delta(\tau - \tau', \mathbf{x} - \mathbf{x}')$ which is given by Eq. (2.60) over the chosen contour.[10] The propagator is periodic in τ over a period β as imposed by the KMS-condition (Eq. (2.57)), which is a straightforward verification. Completion of the square of the free Lagrangian renders the generating functional in the form

$$Z_0[j] = Z_0[0] \exp\left[\frac{1}{2} \iint_0^\beta \mathrm{d}\tau\, \mathrm{d}\tau' \iint \mathrm{d}^3x\, \mathrm{d}^3x'\, j(\tau, \mathbf{x}) \Delta(\tau - \tau', \mathbf{x} - \mathbf{x}') j(\tau', \mathbf{x}')\right]. \tag{2.67}$$

Comparing with Eq. (2.34), the *Euclidean propagator* of a neutral scalar may be found as

$$i D_{\mathrm{E}}(-i\tau, \mathbf{x}) \equiv \Delta(\tau, \mathbf{x}). \tag{2.68}$$

Note the purely imaginary temporal coordinate of the Euclidean propagator. $Z_0[j]$ shown above generates all the Green's functions with imaginary-time arguments.

The above results are analogous to zero-temperature theory with the two differences that

- the temporal integration is reduced to the periodic interval $[0, \beta]$:
$i \int \mathrm{d}t \to \int_0^\beta \mathrm{d}\tau$.

- the free propagator of a scalar field is no longer the Feynman propagator but the thermal propagator of Matsubara:
$D_{\mathrm{F}}(x - x') \to \Delta(\tau - \tau', \mathbf{x} - \mathbf{x}')$.

Due to the periodicity condition (antiperiodicity for fermionic fields) applied to the bosonic fields, and therefore on the thermal propagator, over β, the Matsubara propagator may be written in Fourier space as a sum over discrete frequencies ω_n. Transformation of Eq. (2.38) using the Matsubara contour leads to

$$\Delta(\tau - \tau', \mathbf{x} - \mathbf{x}') = \frac{1}{\beta} \sum_n \int \frac{\mathrm{d}^3k}{(2\pi)^3} e^{-i\omega_n(\tau - \tau') + i\mathbf{k}\cdot(\mathbf{x} - \mathbf{x}')} \frac{1}{\omega_n^2 + \omega_{\mathbf{k}}^2} \tag{2.69}$$

with $\omega_n = 2n\pi/\beta$ (bosonic), $\omega_n = (2n+1)\pi/\beta$ (fermionic), and $\omega_{\mathbf{k}}^2 = |\mathbf{k}|^2 + m^2$. Note that $\omega_{\mathbf{k}} \equiv \omega(|\mathbf{k}|)$, meaning that $\mathbf{k}$ denotes an argument of the function rather than an index to be summed over. The ω_n's are the *Matsubara frequencies* and they parametrise an infinite number of poles of the momentum-space propagator located on the imaginary axis since

$$\tilde{\Delta}(i\omega_n, \mathbf{k}) = \frac{1}{\omega_n^2 + \omega_{\mathbf{k}}^2} \equiv \int \frac{\mathrm{d}k_0}{2\pi} \frac{\rho_0(k)}{k_0 - i\omega_n}. \tag{2.70}$$

To obtain an expression analogous to zero-temperature theory, define $k_0 = i\omega_n$ in Eq. (2.69). Then

$$i D_E(x - x') = -\frac{1}{\beta} \sum_n \int \frac{\mathrm{d}^3k}{(2\pi)^3} e^{-k\cdot(x - x')} \frac{1}{k^2 - m^2} \tag{2.71}$$

where the energy coordinates k_0 are purely imaginary.

---

[10]On the Matsubara contour, the propagator may be expressed in terms of the real variable τ so that $t - t' \to \tau - \tau'$ and $\Theta_C(t - t') \to \Theta(\tau - \tau')$.

2.4.3   The imaginary-time Feynman rules

In the path-integral formulation, the generating functional may be expanded to yield the Feynman rules of the imaginary-time formalism through a perturbative series. Following the reasoning of Sec. 2.2.4, the Euclidean action may be split into a quadratic free part and an interaction part so that $S_\mathrm{E} = S_0 + S_\mathrm{I}$. The generating functional of Eq. (2.32) may then be expanded as

$$
\begin{aligned}
Z[j] &= \mathcal{N} \int [\mathcal{D}\phi]\, e^{-S_0} e^{-S_\mathrm{I} + j \cdot \phi} \\
&= \mathcal{N} \int [\mathcal{D}\phi]\, e^{-S_0} \left\{ 1 + \left(-S_\mathrm{I} + j \cdot \phi \right) + \tfrac{1}{2} \left(-S_\mathrm{I} + j \cdot \phi \right)^2 + \dots \right\}.
\end{aligned}
\tag{2.72}
$$

Each term in this series may be interpreted as a statistical average with respect to $\exp[-S_0]$ so that

$$
Z[j] = Z_0[0] \left\{ 1 + \langle (-S_\mathrm{I} + j \cdot \phi) \rangle_0 + \tfrac{1}{2} \langle (-S_\mathrm{I} + j \cdot \phi)^2 \rangle_0 + \dots \right\}.
\tag{2.73}
$$

The Feynman rules are extracted from this series. For the specific case of ϕ^l-theory with a coupling constant λ, the rules are given as follows:

- Draw diagrams using Wick contractions and determine symmetry factors.

- Define $k_0 = i\omega_n$ and assign a propagator $\tilde{\Delta}(k)$ to each line and a factor of $-\lambda$ to each vertex i.

- Impose energy-momentum conservation through $\beta(2\pi)^3\, \delta_{n0} \delta^{(3)} \left(\sum_i \mathbf{k}_i \right)$ with $n = \sum_i n_i$. A global conservation factor $\beta(2\pi)^3 \delta_{00} \delta^{(3)}(0)$ may be separated out corresponding to the exclusion of one vertex.

- Sum and integrate over all internal energies and momenta k_i: $\frac{1}{\beta} \sum_n \int \frac{\mathrm{d}^3 \mathbf{k}_i}{(2\pi)^3}$.

Further, the definition of the cumulant (Eq. (2.44)) allows for the extraction of connected diagrams with at least one external leg so that

$$
\log Z[j] = \log Z[0] + \langle e^{-S_\mathrm{I}} (e^{j \cdot \phi} - 1) \rangle_\mathrm{con}.
\tag{2.74}
$$

2.4.4   Frequency summation and pinch singularities

In the loops of the diagrammatic expansion of the Matsubara formalism, one must perform the energy summation over thermal functions of the discrete Matsubara frequencies. This is commonly performed by analytic continuation of the summation away from the discrete frequencies and down to the real axis. The procedure, outlined in [12], allows for the replacement of the energy summation by closed integrals due to Cauchy's theorem. However, while the continuation of the summation procedure is well described, the diagrammatic product of Matsubara propagators that occur under the summation must be continued as well. The details of this continuation will be discussed below in Sec. 2.6 when considering self-energies but the procedure often introduces divergencies, so-called *pinch singularities*, briefly mentioned here. Pinch singularities arise when products of continued propagators appear in the form

$$
\frac{1}{k_0^2 - \omega_\mathbf{k}^2 + i\epsilon} \frac{1}{k_0^2 - \omega_\mathbf{k}^2 - i\epsilon}.
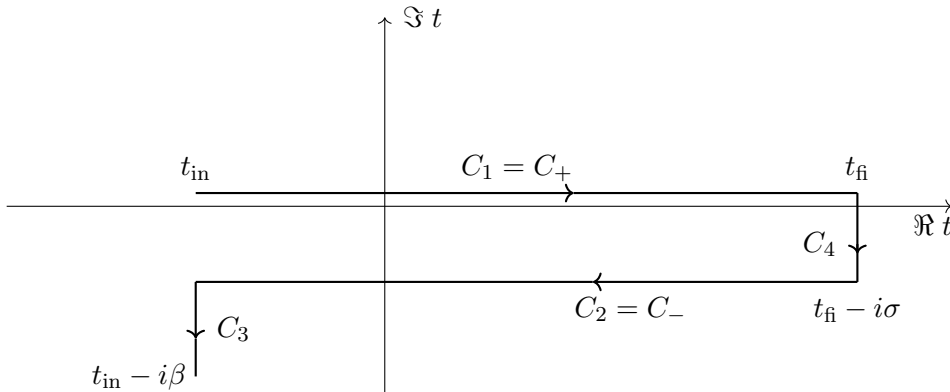\tag{2.75}
$$

Figure 3: **A generalised Keldysh contour** $C = C_1 \cup C_2 \cup C_3 \cup C_4$**.** The contour is extended along the real axis in order to go through the real time arguments of the n-point function of interest. It then goes down by $i\sigma$ before going back parallel to the real axis. Finally, the contour goes down to the final time $t_{\text{in}} - i\beta$. The points t_{in} and t_{fi} are arbitrary and may be suitably chosen for any system.

In the limit when $\epsilon \to 0^+$, the contour of integration is 'pinched' between the poles and the integration becomes ill-defined. Such singularities usually arise at higher-loop orders and must be regulated in order to assign meaning to observables.

2.5 The real-time formalism

Matsubara found that, by the procedure of analytic continuation of Euclidean Green's functions, retarded correlation functions of real time-arguments, and hence observables, may be obtained in the imaginary time formalism presented above. However, the evaluation of momentum integrals over Matsubara propagators is by no means straightforward for any but the simplest cases. By calculating Green's functions in the *real-time formalism*, analytic continuation is avoided completely and this formalism is free of the pinch singularities that appear in the continuation process of Matsubara. The real-time procedure is originally due to Schwinger [21] and Keldysh [8]. The formalism makes use of a special contour of temporal integration, the *Keldysh contour* presented in Fig. 2, which has the effect of doubling the degrees of freedom. This results in a 2×2-matrix structure of the propagator.

2.5.1 The real-time contour

The Keldysh contour of Fig. 2 is a special case of a family of real-time Keldysh-esque contours [9, 22] parametrised by $\sigma \in [0, \beta]$ and presented in Fig. 3. The Keldysh contour is recovered for $\sigma = 0$. An even more general family of contours was presented in [22] with pieces going back and forth N times between $\Re\, t_{\text{in}}$ and $\Re\, t_{\text{fi}}$ in parallel to the real axis. However, it can be shown that such additional pieces cancel out for $N \geq 2$. Fundamental reasons for discarding this extended class of contours are laid out in [22]. Hence, the contour presented in Fig. 3 is the most general real-time contour that includes all n-point functions with real arguments, with σ being a freedom of choice. Commonly, this parameter is set to 0, β or $\beta/2$ [11,12,16,23].

It was argued previously, using Eqs. (2.60) and (2.59), that the contour propagator depends explicitly on the choice of contour. It is clear from these equations that the contour

dependence of the propagator enters only through the contour step-function $\Theta_C(t - t')$. In the case of the real-time contour of Fig. 3, the time coordinates of x, x' may be distributed arbitrarily over C and several unique two-point functions (propagators) arise. Label t_r, t'_s so that $t_r \in C_r$, $t'_s \in C_s$ for $r, s = \{1, 2, 3, 4\}$. Then the different propagators may be expressed as

$$D^{rs}(t - t') = D_C(t_r - t'_s). \tag{2.76}$$

Note e.g. that t_2, t_3 always are later than t_1, t_4. The appearance of several distinct propagators is a very general consequence of the statistical formulation of the two-point function of Eq. (2.16). The Keldysh contour of Fig. 2 is treated in great detail by Wagner [15]. In an approach valid both in as well as out of equilibrium, Wagner organised the two-point functions (Green's functions) in a matrix. In the special case of $\sigma = 0$, this matrix is

$$\mathbf{D}(t, t') = \begin{pmatrix} D^{11}(t, t') & D^{12}(t, t') & D^{13}(t, t') \\ D^{21}(t, t') & D^{22}(t, t') & D^{23}(t, t') \\ D^{31}(t, t') & D^{32}(t, t') & D^{33}(t, t') \end{pmatrix}. \tag{2.77}$$

Adding the piece C_4 ($\sigma = 0$) is a trivial extension. In the limit $t_{\text{in}} \to -\infty$ and $t_{\text{fi}} \to +\infty$, for any system in equilibrium, Landsman and van Weert [12] and Wagner [15] argued that the contour pieces C_3, C_4 decouple entirely from the parallel pieces in the sense that

$$D^{rs}(t - t') = 0 \qquad \text{if } \big(r = 1, 2 \,\wedge\, s = 3, 4\big) \,\vee\, \big(r = 3, 4 \,\wedge\, s = 1, 2\big). \tag{2.78}$$

This may be proven by the application of the Riemann-Lebesgue lemma [24] if the source field is constrained to

$$\lim_{t \to \pm\infty} j(x) = 0. \tag{2.79}$$

This condition is compatible with the KMS condition [12]. A consequence of the decoupling of the vertical contour segments is that the generating functional factorises as

$$Z[j] = Z[0] Z_{34}[j] Z_{12}[j] \tag{2.80}$$

with

$$Z_{rs}[j] = \exp\left[i \int_{C_{rs}} \mathrm{d}^4 x \, \mathcal{L}_{\text{I}}\left[\frac{\delta}{i\delta j(x)}\right]\right] \exp\left[-\frac{i}{2} \int_{C_{rs}} \mathrm{d}^4 x \int_{C_{rs}} \mathrm{d}^4 x' \, j(x) D_C(x - x') j(x')\right]. \tag{2.81}$$

Here, $C_{rs} = C_r \cup C_s$. Therefore, the main concern, when considering real-time Green's functions, is the upper left 2×2-corner of the matrix in Eq. (2.77).

2.5.2 The real-time propagator

The explicit real-time thermal propagator of a neutral scalar particle can be found by examining Eq. (2.81) in the light of Eq. (2.80). Having factorised out the vacuum bubbles $Z[0]$ and the vertical contour pieces $Z_{34}[j]$, only the real-time part $Z_{12}[j]$ will be considered from here on. The two exponentials in $Z_{12}[j]$ can be further factorised with respect to $C_1 \cup C_2$ by conveniently organising the propagator components in a matrix. From now on, the spatial variables will be suppressed. At the same time, a new notation will be introduced. The contour pieces C_1, C_2 of Fig. 3 are relabelled C_+, C_- respectively to indicate chronological

and antichronological time evolution on the different parts of the contour. The factorisation of the first exponential becomes

$$\exp\left[i\int_{C_{+-}}\mathrm{d}t\,\mathcal{L}_\mathrm{I}\left[\frac{\delta}{i\delta j(t)}\right]\right]=\exp\left[i\int_\mathbb{R}\mathrm{d}t\left(\mathcal{L}_\mathrm{I}\left[\frac{\delta}{i\delta j_+(t)}\right]-\mathcal{L}_\mathrm{I}\left[\frac{\delta}{i\delta j_-(t)}\right]\right)\right]. \qquad (2.82)$$

The relative minus sign is a result of the antichronological evolution of the fields on C_-. The two fields $j_+(t)$, $j_-(t)$ are introduced as sources of two separate field components ϕ_+, ϕ_- that exist only on C_+, C_- respectively. Together, the components form the full real-time field $\phi=\begin{pmatrix}\phi_+ & \phi_-\end{pmatrix}^\mathrm{T}$. The physical field component ϕ_+ evolves chronologically and its integration limits are recognised from zero-temperature field theory. The component ϕ_- is an unphysical degree of freedom since it evolves antichronologically. This field component can not appear on external lines of diagrams generated by the above exponential. Nevertheless, its presence is an unavoidable consequence of the Keldysh contour, and contributions from virtual ϕ_--fields in loops must be taken into account. Such contributions are introduced by the second term $\mathcal{L}_\mathrm{I}[\delta/i\delta j_-]$. Summing over $r,s=\pm$, the second exponential factor can be rewritten as

$$\exp\left[-\frac{i}{2}\iint_{C_{rs}}\mathrm{d}t\,\mathrm{d}t'\,j(t)D_C(t-t')j(t')\right]=\exp\left[-\frac{i}{2}\iint_{\mathbb{R}^2}\mathrm{d}t\,\mathrm{d}t'\,j_r(t)D^{rs}(t-t')j_s(t')\right]. \qquad (2.83)$$

The matrix components of the propagator must fulfil

$$\begin{cases}D^{(++)}(t-t')\equiv D_C(t-t'), \\ D^{(--)}(t-t')\equiv D_C\big((t-i\sigma)-(t'-i\sigma)\big)\equiv-\big[D^{(++)}(t-t')\big]^*, \\ D^{(+-)}(t-t')\equiv D_C\big(t-(t'-i\sigma)\big), \\ D^{(-+)}(t-t')\equiv D_C\big((t-i\sigma)-t'\big).\end{cases} \qquad (2.84)$$

The right-most side of the second line reflects the negative orientation of C_2 and can be show explicitly from, for example, Eq. (2.92). These components may be used to express the general propagator of Eq. (2.59) for any bosonic or fermionic field of arbitrary spin and any charge. The explicit solution of Eq. (2.59) for each of the above components gives, after a Fourier transform of Eq. (2.60),

$$\begin{cases}i\tilde{D}^{(++)}_{\alpha\beta}(k)=\big[\Theta(k_0)i\tilde{\Delta}_F(k)+\Theta(-k_0)i\tilde{\Delta}_F^*(k)+\eta\rho_0(k)n(\omega_+)\big]d_{\alpha\beta}(k), \\ i\tilde{D}^{(--)}_{\alpha\beta}(k)=\big[i\tilde{D}^{(++)}(k)\big]^*d_{\alpha\beta}(k), \\ i\tilde{D}^{(+-)}_{\alpha\beta}(k)=\eta\rho_0(k)e^{\sigma k_0}n(\omega_+)d_{\alpha\beta}(k), \\ i\tilde{D}^{(-+)}_{\alpha\beta}(k)=\eta e^{\mp\beta\mu}e^{(\beta-2\sigma)k_0}\cdot i\tilde{D}^{(+-)}_{\alpha\beta}(k).\end{cases} \qquad (2.85)$$

Here, the internal indices i, j have been suppressed and

$$i\tilde{\Delta}_F(k)=\frac{i}{k^2-m^2+i\epsilon} \qquad (2.86)$$

is the Feynman propagator of zero-temperature theory. Recall that the spectral density ρ_0 is the discontinuity over the real axis of this propagator (Eq. (2.39)) and may therefore also be written in terms of $i\tilde{\Delta}_F$, $i\tilde{\Delta}_F^*$ as

$$\rho_0(k)=\mathrm{sign}(k_0)\big[i\tilde{\Delta}_F(k)-i\tilde{\Delta}_F^*(k)\big]. \qquad (2.87)$$

Hence, the propagator matrix may be diagonalised in a basis of zero-temperature functions by means of a Bogolyubov transformation. The result is

$$i\tilde{\mathbf{D}}_{\alpha\beta}(k) = \mathbf{M}_\eta(k) \begin{pmatrix} d_{\alpha\beta}(k)i\tilde{\Delta}_F(k) & 0 \\ 0 & -d_{\alpha\beta}(k)i\tilde{\Delta}_F^*(k) \end{pmatrix} \mathbf{M}_\eta(k) \tag{2.88}$$

with the thermal (Bogolyubov) matrix

$$\mathbf{M}_\eta(k) = \begin{pmatrix} \cos[\text{h}]\theta_k & \eta e^{\beta\mu/2}e^{-(\beta-2\sigma)k_0/2}\sin[\text{h}]\theta_k \\ e^{-\beta\mu/2}e^{(\beta-2\sigma)k_0/2}\sin[\text{h}]\theta_k & \cos[\text{h}]\theta_k \end{pmatrix}. \tag{2.89}$$

Here the thermal angle θ_k was introduced[11] through the functions

$$\begin{cases} \sin[\text{h}]\theta_k = \sqrt{N(\omega)}, \\ \cos[\text{h}]\theta_k = \left[\Theta(k_0) + \eta\Theta(-k_0)\right]\sqrt{1+\eta N(\omega)}, \end{cases} \quad \text{for fermionic[bosonic] fields.} \tag{2.90}$$

The thermal function is $N(\omega) = \Theta(k_0)n(\omega_+) + \Theta(-k_0)n(-\omega_+)$. The square-parenthesis notation conveys that for fermions the goniometric functions are assumed while the hyperbolic functions apply to the scalar case. Note that the propagator is symmetric under simultaneous transposition and reversal of momentum, i.e. $i\tilde{D}^{rs}(k) = i\tilde{D}^{sr}(-k)$, for neutral bosons.[12] For $T = 0$, the Bogolyubov matrix becomes the unit matrix. In that case, the field components completely decouple in the sense that $Z_{+-} \to Z_+Z_-$ and the contribution from ϕ_- may be completely absorbed into the irrelevant normalisation constant. The diagonalisation of the propagator is particularly useful since any thermal dependence may be absorbed into vertices leaving a basis where the propagator itself is defined in terms of zero-temperature functions. Hence, the real-time formalism and the propagator is intrinsically connected to the imaginary-time formalism since they meet when the formalism of Matsubara is analytically continued. This statement is formulated as

$$i\tilde{D}^{(++)}(k) = i\tilde{D}(k) \equiv n(\omega_+)i\Delta(k_0 - i\epsilon, \mathbf{k}) - [1 + n(\omega_+)]i\Delta(k_0 + i\epsilon, \mathbf{k}) \tag{2.91}$$

where Δ is the analytic continuation to the real axis of the Matsubara propagator of Eq. (2.69) with $k_0 = \omega_n \to k_0 \in \mathbb{R}$. The second equality take in the propagator of Eq. (2.41).

2.5.3   The real-time scalar propagator(s)

The thermal decays of interest to this work involve interactions between fermions and scalar bosons. In this subsection and the one that follows, the real-time free propagators for such fields will be presented. First, for the scalar field (commuting or anticommuting), in which case the Klein-Gordon divisor $d_{\alpha\beta}(k)$ is equal to unity. For the choice of $\sigma = 0$, the components of Eq. (2.85) may be written as

$$\begin{cases} i\tilde{D}^{(++)}(k) = \dfrac{i}{k^2 - m^2 + ik_0\epsilon} + \eta\rho_0(k)n(\omega_+), \\ i\tilde{D}^{(--)}(k) = \dfrac{-i}{k^2 - m^2 - ik_0\epsilon} + \eta\rho_0(k)n(\omega_+), \\ i\tilde{D}^{(+-)}(k) = \eta\rho_0(k)n(\omega_+), \\ i\tilde{D}^{(-+)}(k) = \rho_0(k)e^{\omega_+}n(\omega_+). \end{cases} \tag{2.92}$$

---

[11]This diagonalisation procedure was first formulated by Umezawa, Matsumoto and Tachiki [25] in the framework of thermo field dynamics.

[12]Neutral bosons have $\eta = +1$, $\mu = 0$ and $d_{\alpha\beta}(k) = 1$

One recognises the retarded and advanced propagators

$$i\tilde{D}^R(k) = \frac{i}{k^2-m^2+ik_0\epsilon}, \qquad i\tilde{D}^A(k) = \frac{-i}{k^2-m^2-ik_0\epsilon} \tag{2.93}$$

from zero-temperature theory. For practical calculations, it is common to rewrite the four components in terms of the Feynman propagator (and its conjugate), consequently rewriting also the thermal terms. Through the relation

$$i\tilde{D}^R(k) = \Theta(k_0)i\tilde{\Delta}_F(k) - \Theta(-k_0)i\tilde{\Delta}_F^*(k) \tag{2.94}$$

and by insertion of the explicit spectral density Eq. (2.39), the components can be found as

$$\begin{cases} i\tilde{D}^{(++)}(k) = \dfrac{i}{k^2-m^2+i\epsilon} + \eta 2\pi\delta(k^2-m^2)\Big[n(|\omega|_+) + n(|\omega|_-)\Big], \\[2mm] i\tilde{D}^{(--)}(k) = \dfrac{-i}{k^2-m^2-i\epsilon} + \eta 2\pi\delta(k^2-m^2)\Big[n(|\omega|_+) + n(|\omega|_-)\Big], \\[2mm] i\tilde{D}^{(+-)}(k) = \eta 2\pi\delta(k^2-m^2)\Big[n(|\omega|_+) - n(-|\omega|_-)\Big], \\[2mm] i\tilde{D}^{(-+)}(k) = -\eta 2\pi\delta(k^2-m^2)\Big[n(-|\omega|_+) - n(|\omega|_-)\Big]. \end{cases} \tag{2.95}$$

Here, the new thermal distributions introduced for compact notation are:

$$n(|\omega|_\pm) = \frac{\Theta(\pm k_0)}{e^{|\omega|_\pm} - \eta}, \qquad |\omega|_\pm = \beta(|k_0| \mp \mu). \tag{2.96}$$

Note especially that, in the case of a neutral boson, one might define

$$n_B(|k_0|) = \Big[n(|\omega|_+) + n(|\omega|_-)\Big]_{\mu=0} \equiv \frac{1}{e^{\beta|k_0|} - 1} \tag{2.97}$$

and, for further future convenience (see Secs. 3-6), in the case of charged fermions

$$n_{F/\bar{F}}(k_0) = n(|\omega|_\pm) + n(|\omega|_\mp) \equiv \frac{\Theta(k_0)}{e^{\beta(|k_0|\mp\mu)} + 1} + \frac{\Theta(-k_0)}{e^{\beta(|k_0|\pm\mu)} + 1}. \tag{2.98}$$

The lower sign reflects the opposite charge of antiparticles.

2.5.4 The real-time spin-$\frac{1}{2}$ propagators

Considering spin-$\frac{1}{2}$ fields, the Klein-Gordon divisor carry spin structure and for fermions (upper sign)/antifermions (lower sign) it is

$$d_{\alpha\beta}(k) \to d_{F/\bar{F}}(k) = (\slashed{k} \pm m). \tag{2.99}$$

Recall that $\eta = -1$ for Fermi-Dirac statistics. The propagator components may then be found from Eq. (2.85) as

$$\begin{cases} i\tilde{S}_{F/\bar{F}}^{(++)}(k) = (\slashed{k} \pm m)\Big\{\dfrac{i}{k^2-m^2+i\epsilon} - 2\pi\delta(k^2-m^2)\,n_{F/\bar{F}}(k_0)\Big\}, \\[2mm] i\tilde{S}_{F/\bar{F}}^{(--)}(k) = (\slashed{k} \pm m)\Big\{\dfrac{-i}{k^2-m^2-i\epsilon} - 2\pi\delta(k^2-m^2)\,n_{F/\bar{F}}(k_0)\Big\}, \\[2mm] i\tilde{S}_{F/\bar{F}}^{(+-)}(k) = -2\pi(\slashed{k} \pm m)\delta(k^2-m^2)\Big[n(|\omega|_\pm) - n(-|\omega|_\mp)\Big], \\[2mm] i\tilde{S}_{F/\bar{F}}^{(-+)}(k) = 2\pi(\slashed{k} \pm m)\delta(k^2-m^2)\Big[n(-|\omega|_\mp) - n(|\omega|_\pm)\Big]. \end{cases} \tag{2.100}$$

In the simple case of neutral particles, with $\mu = 0$, these components reduce to those of Das [26].

2.5.5 Real-time Feynman rules

It was seen in the previous section that the Keldysh contour of Fig. 2 necessarily gives rise to a doubling of the degrees of freedom in the real-time thermal theory. This is expressed by separating the field into two components, each appearing on the respective segments of the real-time contour. One component is physical while the other is to be regarded as a thermal ghost arising from the choice of the specific contour. For notational convenience, a neutral scalar field ϕ will be considered in the derivation of the Feynman rules below. For simplicity, the field is assumed to have an interaction term proportional to $\lambda \phi^l$. The generality of the method, however, allows for the treatment of the multicomponent vector field Φ^i_α introduced above. The derivation of the Feynman rules is analogous for the case of Φ^i_α, only with the addition of contraction of Lorentz and internal indices to the summation over the thermal propagator components.

It was seen in Sec. 2.5.2 that, for a field with no derivative couplings, the relevant factor in the generating functional, $Z_{12}[j]$, can be written as

$$Z_{+-}[j] \to Z[j_+, j_-]$$
$$= \exp\left[i \int_{\mathbb{R}} \mathrm{d}t \left(\mathcal{L}_{\mathrm{I}}\left[\frac{\delta}{i\delta j_+}\right] - \mathcal{L}_{\mathrm{I}}\left[\frac{\delta}{i\delta j_-}\right] \right)\right] \exp\left[-\frac{i}{2} \iint_{\mathbb{R}^2} \mathrm{d}t\, \mathrm{d}t'\, j_r(t) D^{rs}(t - t') j_s(t')\right]. \quad (2.101)$$

The series expansion of this function generates all the diagrams of the theory in analogy to the zero-temperature case. Two distinct vertices appear due to the two interaction terms in the leftmost exponential: one interaction vertex involves only the physical field component and one vertex involves only the ghost field. See Fig. 4 for the vertices of the ϕ^4-theory. Hence, the field components do not mix at vertices. However, due to the non-zero off-diagonal components of the propagator of the Keldysh contour, the fields may propagate into each other.

The connected Green's functions of Eq. (2.43) are generated by functional differentiation according to

$$G^{(n,m)}(t_1, \ldots, t_n, t_{n+1}, \ldots, t_{n+m}) = \left. \frac{\delta^{n+m} \log Z[j_+, j_-]}{i\delta j_+(t_1) \cdots i\delta j_+(t_n) i\delta j_-(t_{n+1}) \cdots i\delta j_-(t_{n+m})} \right|_{\substack{j_+=0 \\ j_-=0}}. \quad (2.102)$$

It is clear that, for any value of $\sigma \neq 0$, *real-time* Green's functions may only be recovered by functional differentiation with respect to the source j_+ since the second contour segment includes no real times. It may be proven [12] that the real-time Green's functions are independent of the parameter σ and, hence, they are given by

$$G^{(n,0)}(t_1, \ldots, t_n) = \left. \frac{\delta^n \log Z[j_+, j_-]}{i\delta j_+(t_1) \cdots i\delta j_+(t_n)} \right|_{\substack{j_+=0 \\ j_-=0}}, \qquad \forall \sigma. \quad (2.103)$$

The thermal ghost field ϕ_- may only propagate as internal lines connecting vertices. These internal lines are generated by functional differentiation with respect to j_- inside $Z[j_+, j_-]$, see Eq. (2.82).

The full set of Feynman rules can easily be extracted through the generating functional in its path-integral form if the Lagrangian is split into its free and interaction parts. Then, in terms of the action, the generating functional may be written as

$$Z[j_+, j_-] = \int [\mathcal{D}\phi_+] \int [\mathcal{D}\phi_-] \exp\left[i \int_{\mathbb{R}} dt \left\{ \phi_r K^{rs} \phi_s + \mathcal{L}_I(\phi_+) - \mathcal{L}_I(\phi_-) + j_r \phi_r \right\}\right]$$

$$= \int [\mathcal{D}\phi_+] \int [\mathcal{D}\phi_-] \, e^{iS_0} \, e^{i(S_I + j \cdot \phi)}, \qquad \text{with } j \cdot \phi = \int_{\mathbb{R}} dt \, j_r \phi_r. \qquad (2.104)$$

Summation over $r, s = \pm$ is assumed. Expanding the second exponential, each term may be interpreted as an expectation value in the path-integral formalism with respect to a weight e^{iS_0} so that

$$Z[j_+, j_-] = \int [\mathcal{D}\phi_+] \int [\mathcal{D}\phi_-] \, e^{iS_0} \left\{ 1 + i\left(S_I + j \cdot \phi\right) + \frac{i^2}{2}\left(S_I + j \cdot \phi\right)^2 + \dots \right\}$$

$$= Z_0[0, 0] \left\{ 1 + i \left\langle (S_I + j \cdot \phi) \right\rangle_0 + \frac{i^2}{2} \left\langle (S_I + j \cdot \phi)^2 \right\rangle_0 + \dots \right\}. \qquad (2.105)$$

By means of the cumulant expansion, it is possible to factor out not only the free $Z_0[0, 0]$ but *all* vacuum bubbles $Z[0, 0]$ so that the cumulant becomes

$$W[j_+, j_-] \equiv \log Z[j_+, j_-] = \log Z[0, 0] + \left\langle e^{iS_I}(e^{ij \cdot \phi} - 1) \right\rangle_{\text{con}}. \qquad (2.106)$$

The expansion of the final term gives all connected diagrams with at least one external leg of the physical field ϕ_+. The real-time Feynman rules are extracted from this series:

- Draw diagrams using ϕ_+-, ϕ_--vertices: n external ϕ_+-lines and arbitrarily many internal ϕ_+- and ϕ_--lines. Determine symmetry factors.

- Connect vertices by assigning a propagator:
  $i\tilde{D}^{rs}(k) = \langle \phi_r \phi_s \rangle_0 = r \text{———} s$.

- Assign a factor of $-i\lambda$ to each ϕ_+-vertex and $i\lambda$ to each ϕ_--vertex.

- Impose energy-momentum conservation at each vertex through $(2\pi)^4 \, \delta^{(4)}\left(\sum_i k_i\right)$. A global conservation factor may be separated out as $(2\pi)^4 \, \delta^{(4)}(0)$.

- Integrate over each internal momentum k_i: $\int \frac{d^4 k}{(2\pi)^4}$ and sum over all internal distributions of r, s.

Comparing the real-time formalism to Matsubara theory, the propagator has gained a matrix structure and, further, two separate types of vertices has appeard.

2.6 Thermal self-energies

This section approaches the goal of expressing the thermal decay rate in terms of the self-energy. Weldon [13] related the self-energy of the Matsubara formalism to the decay rate. In the sections below, we will examine this self-energy, its analytic continuation and finally the connection of real-time quantities to it. This connection has been discussed by several authors, see for example [12, 23, 27].
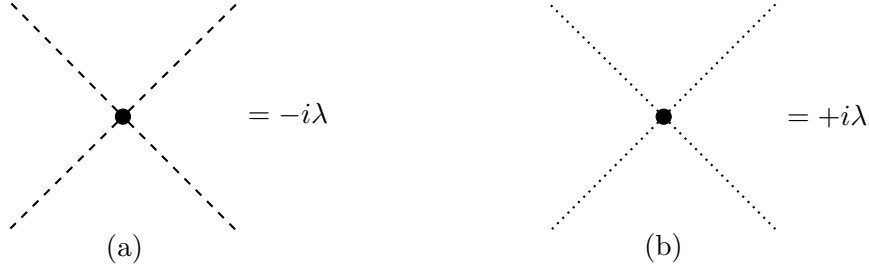
Figure 4: **The two real-time vertices of ϕ^4-theory, appearing on each horisontal piece of the real-time contour respectively.** (a) Vertex corresponding to the quartic interaction of the physical field ϕ_+. (b) Vertex corresponding to the quartic interaction of the unphysical field ϕ_-.

2.6.1 Matsubara formalism

The connected two-point function of the Matsubara formalism is obtained by functional differentiation of the cumulant in Eq. (2.74). In order to obtain a perturbative series, and hence the Feynman rules, in Fourier space, the full generating functional of Eq. (2.73) may be transformed. It may be further manipulated so as to recover a form similar to that of Eq. (2.42). The full propagator appearing in Feynman diagrams is

$$\tilde{G}(k_1, \ldots, k_n) \to (-i)^n \tilde{G}_{\mathrm{E}}(k_1, \ldots, k_n) \tag{2.107}$$

in comparison to the zero-temperature propagator. Since global momentum conservation is imposed, an overall factor of $\beta(2\pi)^3\delta_{n0}\delta\left(\sum \mathbf{k}_i\right)$ may be extracted, leaving the interacting many-body propagator labelled $\tilde{\mathcal{G}}(k)$ by Landsman and van Weert [12]. Analogous to Eq. (2.70), this propagator may be defined as

$$\tilde{\mathcal{G}}(k) = \tilde{\Delta}'(z, \mathbf{k}) = \int \frac{\mathrm{d}k_0}{2\pi} \frac{\rho(k)}{k_0 - z}. \tag{2.108}$$

The free spectral density ρ_0 has been replaced by the corresponding full quantity defined as $i\rho(k) = \mathrm{Disc}\,\tilde{\Delta}'(k)$. This analytic continuation extends the propagator away from the discrete Matsubara frequencies on the imaginary axis and allows the propagator to be defined for real energies. The continuation is not unique and this is usually resolved [12, 17] by letting $\lim_{|z|\to\infty} \tilde{\Delta}'(z, \mathbf{k}) = 0$ and by taking $\tilde{\Delta}'(z, \mathbf{k})$ to be analytic off the real axis. Then uniquely

$$\tilde{\Delta}'(z, \mathbf{k}) = \int_0^\infty \frac{\mathrm{d}(k_0')^2}{2\pi} \frac{\rho(k_0', \mathbf{k})}{z^2 - k_0'^2} \tag{2.109}$$

given that $k_0\rho(k) \geq 0$. This function can be shown to have neither zeroes nor poles off the real axis given this inequality property [12]. Guided by the above definition, it is useful to define the thermal Feynman propagator

$$\tilde{\Delta}'_{\mathrm{F}}(k) = -\tilde{\Delta}'(k_0 + ik_0\epsilon, \mathbf{k}). \tag{2.110}$$

This propagator may be inverted by writing $k_0^2 - |\mathbf{k}|^2 = m^2$ so that the thermal self-energy for the imaginary-time formalism can be extracted:

$$\tilde{\Delta}_{\mathrm{F}}'^{-1} = k^2 - m^2 - \bar{\Pi}_{\mathrm{F}}(k). \tag{2.111}$$

As in zero-temperature theory, one may observe that the real part of the self-energy may be absorbed as a correction to the mass while its imaginary component will be interpreted as a decay rate [13].

2.6.2 Real-time formalism

The full real-time propagator may be assumed to satisfy the Schwinger-Dyson equation (see further references in [12]) similar to the zero-temperature case:

$$\tilde{\mathcal{D}}^{rs}_{\alpha\beta}(k) = \tilde{\mathbf{D}}^{rs}_{\alpha\beta}(k) + \left(\tilde{\mathbf{D}}\tilde{\mathbf{\Pi}}\tilde{\mathcal{D}}\right)^{rs}_{\alpha\beta}(k). \tag{2.112}$$

Like in zero-temperature theory, the real-time self-energy is most often the sum of all one-particle irreducible (1PI)[13] insertions on the propagator line as visualised in Fig. 5.
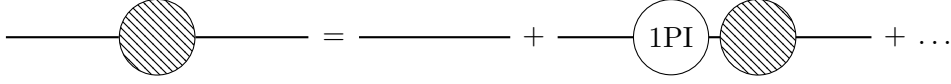

Figure 5: **The graphical interpretation of the Schwinger-Dyson equation.** All 1PI insertions are parametrised by the self-energy. By recursive insertion of the full propagator, the 1PI series expansion may be obtained.

2.6.3 Self-energy relations

Viewing the free-field propagator of Eq. (2.85) as a special case of the full propagator of Eq. (2.112), the matrix of Eq. (2.89) also diagonalises the full propagator for some function $\tilde{\mathcal{D}}_{F\alpha\beta}(k) = \tilde{D}_{F\alpha\beta}(k) + \left(\tilde{D}_F\bar{\Pi}_F\tilde{D}_F\right)_{\alpha\beta}$ so that

$$\tilde{\mathcal{D}}_{\alpha\beta}(k) = \mathbf{M}_\eta \begin{pmatrix} \tilde{\mathcal{D}}_{F\alpha\beta} & 0 \\ 0 & \tilde{\mathcal{D}}^*_{F\alpha\beta} \end{pmatrix} \mathbf{M}_\eta. \tag{2.113}$$

The insertion of $\mathbf{M}_\eta$ and its inverse in the Schwinger-Dyson equation allows for the identification

$$\tilde{\mathbf{\Pi}} = \begin{pmatrix} \tilde{\Pi}^{(++)} & \tilde{\Pi}^{(+-)} \\ \tilde{\Pi}^{(-+)} & \tilde{\Pi}^{(--)} \end{pmatrix} \equiv \mathbf{M}_\eta^{-1} \begin{pmatrix} \bar{\Pi}_F & 0 \\ 0 & -\bar{\Pi}^*_F \end{pmatrix} \mathbf{M}_\eta^{-1}. \tag{2.114}$$

The derivation is rather lengthy but can be found in [12] where it is shown that $\bar{\Pi}_F$ is indeed the analytically continued self-energy of the re-summed propagator $\tilde{\Delta}'_F$ in Eq. (2.111). For notational convenience, possible spinor and Lorentz indices have been suppressed but are generally present in the form of the Klein-Gordon divisor $d^{ij}_{\alpha\beta}$. By inserting the explicit expression for the thermal matrix, the following relations may be deduced:

$$\tilde{\Pi}^{(--)} = -\left[\tilde{\Pi}^{(++)}\right]^*, \tag{2.115}$$

$$\tilde{\Pi}^{(+-)} = \eta e^{-\beta\mu} e^{(\beta-2\sigma)k_0} \tilde{\Pi}^{(+-)}. \tag{2.116}$$

---

[13]A 1PI diagram is defined to be any diagram that cannot be split into two by removal of a single propagator line. The 1PI blob of Fig. 5 is defined as the sum of all such diagrams with the eye-diagram (the single loop) being the lowest order contribution. See [1] for a discussion of the 1PI insertion procedure.

Hence, the number of independent components is less than the initial four. The two relations above hold for any σ, also for $\sigma = 0$. Importantly for the forthcoming calculations, the real and imaginary parts are related as

$$\Re \, \tilde{\Pi}^{(++)} = \Re \, \bar{\Pi}_{\mathrm{F}}, \tag{2.117}$$

$$\Im \, \tilde{\Pi}^{(++)} = \mathrm{sign}(k_0)\big[1 + 2\eta n(\omega_+)\big]\Im \, \bar{\Pi}_{\mathrm{F}}. \tag{2.118}$$

The self-energy on the left-hand side will be calculated to first order for several interaction terms in Secs. 3-6.

2.7 Thermal decay rates

Below, the self-energies of the previous section will be related to the thermal decay rate. Initially, a relation between the corresponding thermal quantity to the zero-temperature decay rate and the self-energy of the imaginary-time formalism due to Weldon [13] will be presented. This relation will then be restated in terms of the self-energy of the real-time formalism by making use of the self-energy relations of Sec. 2.6.3.

2.7.1 Imaginary-time self-energy

The decay rate γ_D for a given process in zero-temperature theory may be related to the discontinuity (the imaginary part) of the self-energy through the optical theorem as

$$\gamma_D = -\left(\frac{\Im \, \Pi_0(E_0)}{E_0}\right), \tag{2.119}$$

where E_0 is the energy of the decaying particle. Weldon [13] defined a similar quantity $\Gamma(p_0)$ so that

$$\Gamma(p_0) = -\left(\frac{\Im \, \bar{\Pi}_{\mathrm{F}}(p_0)}{p_0}\right), \tag{2.120}$$

where $\bar{\Pi}_{\mathrm{F}}$ is the self-energy of the imaginary-time formalism. It is important to understand what this quantity describes. One may assume that the distribution of a particle Φ at some time t_{in} is described by a nonequilibrium function, which Weldon labelled $f(p_0, t_{\mathrm{in}})$ [13]. This function will approach the thermal distribution of the equilibrium (Bose-Einstein or Fermi-Dirac) in a simple manner if the perturbation from equilibrium is small ($\partial f / \partial t \ll 1$). The rate of approach to first order is parametrised by $\Gamma(p_0)$. Weldon formulated the evolution of this distribution as

$$\frac{\partial f}{\partial t} = -f\Gamma_D + (1 + \eta f)\Gamma_I. \tag{2.121}$$

What does this mean? The first term simply expresses the loss of Φ-particles through decay modes while Γ_I takes into account that the medium is not empty. Rather, the thermal medium is filled with particles that couple to Φ and, hence, this second parameter, the *inverse decay rate* (production rate), adds the contribution from processes in the medium that produce Φ particles. As an example, production may occur through reactions $\phi^1\phi^2 \to \Phi$. Weldon comprehensively presents an analysis of possible production and decay channels for Φ through interactions with medium particles.

The solution to Eq. (2.121) is

$$f(p_0, t) = n(\omega_+) + c(p_0)e^{-\Gamma(p_0)t}. \tag{2.122}$$

This solution requires that the temperature T is constant over time. Since T characterises the background medium, the perturbations of the distribution of Φ must be small and one may assume that the distribution of the medium particles is the thermal equilibrium distribution. The net decay rate Γ of the distribution of Φ in the medium is the rate at which the distribution of Φ approaches the equilibrium function and it is

$$\Gamma(p_0) = \Gamma_D - \eta\Gamma_I. \tag{2.123}$$

The evaluation of the amplitude for the thermal forward decay Γ_D is of interest in this thesis work. Fortunately, Weldon provides a thermal relation between the forward and inverse decay rates due to unitarity so that one therefore may write the decay rate of Φ as

$$\Gamma_D = -\frac{1}{1 - \eta e^{-\beta(p_0-\mu)}}\frac{\Im\,\bar{\Pi}_{\mathrm{F}}(p_0)}{p_0}. \tag{2.124}$$

For the purpose of this work, the expression provided by Weldon has here been extended in order to explicitly include the chemical potential μ.

2.7.2   Real-time self-energy

The self-energy relations of Sec. 2.6.3 related the self-energy of the imaginary-time formalism to the components of the real-time self-energy. Eq. (2.124) may hence be written as

$$\Gamma_D = -\mathrm{sign}(p_0)\frac{1 + \eta n(\omega_+)}{1 + 2\eta n(\omega_+)}\frac{\Im\,\tilde{\Pi}^{(++)}(p_0)}{p_0}. \tag{2.125}$$

In the following sections 3-6, the $(++)$-component of several real-time self-energies is presented to first order as the self-energy of the eye-diagram. The results are used for extracting predicted decay rates for fields in an equilibrated thermal medium.

Note that, if $\tilde{\Pi}^{(++)}$ comes with internal or Lorentz indices, one may follow the procedure advised by Weldon [13] and define the scalar function

$$\Sigma(p) = \bar{\Phi}^i_\alpha(p)\tilde{\Pi}^{(++)\,ij}_{\alpha\beta}(p)\Phi^j_\beta(p), \tag{2.126}$$

which is the contraction with asymptotic states. This allows for a probabilistic interpretation of Σ as the decay rate, similar to a Breit-Wigner resonance, for any particle species.

For convenience, the ratio of the thermal decay rate above to the zero-temperature limit may be defined:

$$R = \frac{\Gamma_D}{\gamma_D}. \tag{2.127}$$

If this ratio is equal to unity for all temperatures, the medium has no effect on decay rates.

3   (Pseudo)scalar decay into (pseudo)scalars

We now have the formalism and the relations needed to compute thermal decay rates. This section presents the thermal rate at which a neutral (pseudo)scalar particle Φ of mass M decays into a neutral (pseudo)scalar pair $\phi^1\phi^2$ of masses m_1, m_2 as a result of calculations performed within the thesis work. The scalars in the final state need not to be identical in
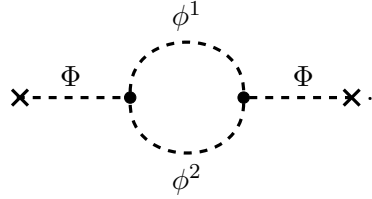
the following calculations. Note, however, that all scalars considered are neutral particles. The model responsible for such a decay process contains the interaction term

$$\mathcal{L}_{\text{int}} = \lambda \Phi \phi^1 \phi^2. \tag{3.1}$$

The resulting self-energy of this section has been published in [23] but the full calculation was performed independently within this work as an introductory example.

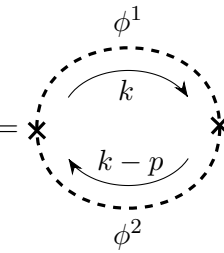## 3.1   The real-time self-energy of the scalar-scalar eye-diagram

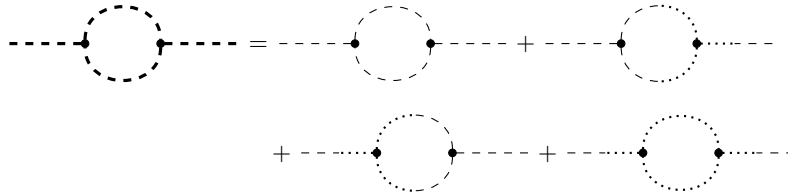Using the interaction term of Eq. (3.1), one may draw the following eye-diagram:

$$\tag{3.2}$$

This is the matrix eye-diagram appearing in the Dyson series that expresses the full interacting propagator of Φ. The crosses denote either external legs or connections to vertices. The Φ-lines are amputated in the following self-energy calculation for the loop. It is clear that the intermediate scalars ϕ^1, ϕ^2 are virtual and their momenta must be integrated out. Note that this diagram represents all allowed propagator combinations.[14] The intermediate particles are not restricted to the physical field component ϕ_+ but the external legs are. As a consequence, all valid combinations of propagators must be considered when calculating the total amplitude for this diagram. Only the physical field component may appear on the external legs and, in the primary basis used in this thesis, $(+)$- and $(-)$-field components do not mix at vertices, cf. Fig. 4. Each vertex contributes with a factor of $\mp i\lambda$. Note that the pseudoscalar loop is identical to the scalar-scalar loop.

In order to obtain the thermal decay rate, the self-energy of Eq. (3.2) will be calculated in the following. This self-energy is defined as the bubble

$$i\mathcal{I}_{\text{bubble}}(p; m_1, m_2) = \tag{3.3}$$

---

[14]The thick lines are drawn in order to indicate the free matrix propagator. Hence, the diagram represents the sum of diagrams over all valid combinations of ϕ_+, ϕ_-. Note that only the physical field component ϕ_+ may appear on external lines.

The crosses are vertices connected to external legs in the case of interest to this thesis. All components of this self-energy are related through Eq. (2.114) and the evaluation of the $(++)$-component is sufficient in order to calculate the decay rate. This component is

$$
i\mathcal{I}_{\text{bubble}}^{(++)}(p; m_1, m_2)
$$
$$
= i(1 + \delta_{12})(-i\lambda)^2 \int \frac{\mathrm{d}^4 k}{(2\pi)^4} i\tilde{D}^{(++)}(k - p; m_1) i\tilde{D}^{(++)}(k; m_2)
$$
$$
= iI_{\text{SS}}^{(2)}(p^2; m_1, m_2) + \left[iF_{\text{SS}}^{(2)}(p; m_1, m_2) + (1 \leftrightarrow 2) \right] + iF_{\text{SS}}^{(3)}(p; m_1, m_2). \tag{3.4}
$$

Note here the pre-factor; δ_{12} is defined as unity if the two particles in the loop are of the same species and zero otherwise. Hence, the correct symmetry factor will be taken into account when considering either identical or distinct loop particle species.[15] The two-component structure of the scalar propagator splits the bubble into four terms above; a non-thermal (temperature independent) integral $I_{\text{SS}}^{(2)}$, two mixed integrals $F_{\text{SS}}^{(2)}$ and $(1 \leftrightarrow 2)$, and one purely thermal integral $F_{\text{SS}}^{(3)}$ are defined. The bracketed arrow denotes the interchange of indices 1 and 2 in the second mixed term. The explicit integrals are

$$
iI_{\text{SS}}^{(2)}(p^2; m_1, m_2)
$$
$$
= i(1 + \delta_{12})(-i\lambda)^2 \int \frac{\mathrm{d}^4 k}{(2\pi)^4} \frac{i}{(p - k)^2 - m_1^2 + i\epsilon} \frac{i}{k^2 - m_2^2 + i\epsilon}, \tag{3.5}
$$

$$
iF_{\text{SS}}^{(2)}(p; m_1, m_2)
$$
$$
= i(1 + \delta_{12})(-i\lambda)^2 \int \frac{\mathrm{d}^4 k}{(2\pi)^4} \frac{i}{(p - k)^2 - m_1^2 + i\epsilon} 2\pi\, n_{\text{B}}(|k_0|)\delta(k^2 - m_2^2), \tag{3.6}
$$

$$
iF_{\text{SS}}^{(3)}(p; m_1, m_2)
$$
$$
= i(1 + \delta_{12})(-i\lambda)^2 \int \frac{\mathrm{d}^4 k}{(2\pi)^4} 2\pi\, n_{\text{B}}(|p_0 - k_0|)\delta((p-k)^2 - m_1^2)\, 2\pi\, n_{\text{B}}(|k_0|)\delta(k^2 - m_2^2). \tag{3.7}
$$

3.1.1 The non-thermal self-energy term

The non-thermal contribution to the self-energy is well known from zero-temperature theory, see for example [1]. It may be evaluated by dimensional regularisation techniques in $D = 4 - 2\epsilon$ dimensions at the renormalisation scale μ. The resulting expression for the non-thermal integral is

$$
iI_{\text{SS}}^{(2)}(p^2; m_1, m_2) = (1 + \delta_{12})\frac{\lambda^2}{16\pi^2}\left\{ -\frac{1}{\tilde{\epsilon}} - 2 + \frac{x_+}{2}\ln\left[\frac{m_1^2}{\mu^2}\right] - \frac{x_-}{2}\ln\left[\frac{m_2^2}{\mu^2}\right] - I_{\text{loop}} \right\}. \tag{3.8}
$$

Here, $1/\tilde{\epsilon}$ parametrises the divergence emerging from the dimensional regularisation scheme and, denoting the Euler-Mascheroni constant by γ_{E}, it is defined as $\frac{1}{\tilde{\epsilon}} = \frac{1}{\epsilon} - \gamma_{\text{E}} + \ln 4\pi$. The

---

[15]In the case of identical particles, the symmetry factor of the loop is $S = 2$. However, the vertex factor will gain an additional factor of 2 from identical Wick contractions which later is squared and will after cancellation give the overall factor $1 + \delta_{12}$.

last term I_{loop} is the term of interest to the decay rate since it is complex.

$$
I_{\text{loop}} = \begin{cases}
\dfrac{\sqrt{C}}{2}\left[\ln\left|\dfrac{(\sqrt{C}+x_-)(\sqrt{C}-x_+)}{(\sqrt{C}-x_-)(\sqrt{C}+x_+)}\right| + 2\pi i\right] & \text{if (a)}, \\[2em]
-\sqrt{D}\left[\arctan\dfrac{x_+}{\sqrt{D}} - \arctan\dfrac{x_-}{\sqrt{D}}\right] & \text{if (b)}, \\[2em]
\dfrac{\sqrt{C}}{2}\ln\left|\dfrac{(\sqrt{C}+x_-)(\sqrt{C}-x_+)}{(\sqrt{C}-x_-)(\sqrt{C}+x_+)}\right| & \text{if (c)}.
\end{cases}
\tag{3.9}
$$

The cases are defined as the momentum regions

   a) $p^2 \geq (m_1 + m_2)^2$,

   b) $(m_1 - m_2)^2 \leq p^2 < (m_1 + m_2)^2$,

   c) $p^2 < (m_1 - m_2)^2$,

and

$$
x_\pm = \pm 1 + \frac{m_2^2 - m_1^2}{p^2}, \qquad C = -D = \left(1 - \frac{(m_1 + m_2)^2}{p^2}\right)\left(1 - \frac{(m_1 - m_2)^2}{p^2}\right).
\tag{3.10}
$$

The imaginary part of Eq. (3.8) is

$$
\Im\left[i I_{\text{SS}}^{(2)}(p^2; m_1, m_2)\right] = \begin{cases}
-(1+\delta_{12})\dfrac{\lambda^2}{16\pi}\sqrt{C} & \text{if (a)}, \\[1em]
0 & \text{otherwise}.
\end{cases}
\tag{3.11}
$$

3.1.2   The mixed self-energy term

The mixed self-energy contribution consists of two complex propagator cross terms. The evaluation of the imaginary component of those integrals results in

$$
\Im\left[i F_{\text{SS}}^{(2)}(p; m_1, m_2) + (1 \leftrightarrow 2)\right]
$$

$$
= -(1+\delta_{12})\frac{\lambda^2}{16\pi|\mathbf{p}|\beta}\begin{cases}
\ln\left|\dfrac{1 - e^{-\beta\omega_{2,p_+}}}{1 - e^{-\beta\omega_{2,p_-}}}\right| + (1 \leftrightarrow 2) & \text{if (a)} \ \vee \ \text{(c1)}, \\[1.5em]
0 & \text{if (b)}, \\[1.5em]
-\ln\left|\left(1 - e^{-\beta\omega_{2,p_+}}\right)\left(1 - e^{-\beta\omega_{2,p_-}}\right)\right| + (1 \leftrightarrow 2) & \text{if (c2)}.
\end{cases}
\tag{3.12}
$$

Here

$$
\omega_{2,p_\pm} = \frac{1}{2}\left|p_0\left|1 + \frac{m_2^2 - m_1^2}{p^2}\right| \pm |\mathbf{p}|\sqrt{C}\right|.
\tag{3.13}
$$

Two further cases have been defined as

c1) $0 \leq p^2 < (m_1 - m_2)^2$,

c2) $p^2 < 0$.

The real part of the mixed term is

$$\Re\left[iF_{\mathrm{SS}}^{(2)}(p; m_1, m_2) + (1 \leftrightarrow 2)\right] = (1 + \delta_{12})\frac{\lambda^2}{16\pi^2|\mathbf{p}|}\int_{m_2}^{\infty} d\omega_{2,\mathbf{k}}\, n(\omega_{2,\mathbf{k}})$$

$$\times \mathcal{P}\ln\left|\frac{\left(p^2 - 2p_0\omega_{2,\mathbf{k}} + 2|\mathbf{p}|\sqrt{\omega_{2,\mathbf{k}}^2 - m_2^2} + m_2^2 - m_1^2\right)\left(p^2 + 2p_0\omega_{2,\mathbf{k}} + 2|\mathbf{p}|\sqrt{\omega_{2,\mathbf{k}}^2 - m_2^2} + m_2^2 - m_1^2\right)}{\left(p^2 - 2p_0\omega_{2,\mathbf{k}} - 2|\mathbf{p}|\sqrt{\omega_{2,\mathbf{k}}^2 - m_2^2} + m_2^2 - m_1^2\right)\left(p^2 + 2p_0\omega_{2,\mathbf{k}} - 2|\mathbf{p}|\sqrt{\omega_{2,\mathbf{k}}^2 - m_2^2} + m_2^2 - m_1^2\right)}\right|$$

$$+ (1 \leftrightarrow 2). \tag{3.14}$$

Here $\omega_{2,\mathbf{k}}^2 = |\mathbf{k}|^2 + m_2^2$.

3.1.3 The purely thermal self-energy term

The purely thermal contribution to the self-energy has no real component and was found to be given by the purely imaginary expression

$$iF_{\mathrm{SS}}^{(3)}(p; m_1, m_2) = -i(1 + \delta_{12})\frac{\lambda^2}{8\pi|\mathbf{p}|\beta}\times$$

$$\times \begin{cases} \dfrac{1}{e^{\beta p_0} - 1}\ln\left|\dfrac{\left(1 - e^{-\beta\omega_{2,p_+}}\right)\left(1 - e^{\beta(p_0 - \omega_{2,p_-})}\right)}{\left(1 - e^{-\beta\omega_{2,p_-}}\right)\left(1 - e^{\beta(p_0 - \omega_{2,p_+})}\right)}\right| & \text{if (a),} \\[2em] 0 & \text{if (b),} \\[1.5em] \dfrac{1}{e^{\mp\beta p_0} - 1}\left[\ln\left|\dfrac{1 - e^{-\beta\omega_{2,p_+}}}{1 - e^{-\beta\omega_{2,p_-}}}\right| - e^{\mp\beta p_0}\ln\left|\dfrac{1 - e^{\beta(\pm p_0 - \omega_{2,p_+})}}{1 - e^{\beta(\pm p_0 - \omega_{2,p_-})}}\right|\right] & \text{if (c1)} \wedge \text{(d1),} \\[1.5em] \dfrac{1}{e^{-\beta p_0} - 1}\left[e^{-\beta p_0}\ln\left|1 - e^{\beta(p_0 - \omega_{2,p_\pm})}\right| - \ln\left|1 - e^{-\beta\omega_{2,p_\pm}}\right|\right] & \\[1em] + \dfrac{1}{e^{\beta p_0} - 1}\left[e^{\beta p_0}\ln\left|1 - e^{-\beta(p_0 + \omega_{2,p_\mp})}\right| - \ln\left|1 - e^{-\beta\omega_{2,p_\mp}}\right|\right] & \text{if (c2)} \wedge \text{(d2).} \end{cases} \tag{3.15}$$

The further two cases were defined as

(d1) $m_2 \geq m_1 \ \vee \ m_2 < m_1$.

The leftmost inequality corresponds to the upper sign. The rightmost inequality corresponds to the lower sign.

(d2) $\left\{\left[m_2 \geq m_1 \ \wedge \ 1 + \frac{m_2^2 - m_1^2}{p^2} \geq 0\right] \ \vee \ m_2 < m_1\right\} \vee \left\{m_2 \geq m_1 \ \wedge \ 1 + \frac{m_2^2 - m_1^2}{p^2} < 0\right\}$.

The leftmost curly bracket corresponds to the upper sign. The rightmost curly bracket corresponds to the lower sign.

Note importantly that in the above expression for the purely thermal contribution, the mass parameters m_1, m_2 in $\omega_{2,p_\pm}$ should be replaced by expressions $\min\{m_1, m_2\}$ and $\max\{m_1, m_2\}$ respectively.

The combined $(++)$-self-energy component of the eye-diagram provided in Sec. 3.1.1-3.1.3 is identical to that found by Nishikawa et al. [23] and, thus, their calculation has been verified.

3.1.4 Decay rate of $\Phi \to \phi^1\phi^2$

As mentioned in the beginning of this section, the thermal decay rate of a scalar particle into two scalar particles is identical to that of pseudoscalar particles in the final state. The thermal decay rate of a neutral (pseudo)scalar is given by Eq. (2.125), Sec. 2.7.2. In the special case of identical loop masses, the expression for the self-energy simplifies significantly due to vanishing terms in $\sqrt{C}$ and $\omega_{2,p_\pm}$. The ratio of Eq. (2.127) may be obtained by putting the external particle on-shell in the momentum region $p^2 \geq (m_1 + m_2)^2$ where the zero-temperature decay rate is finite. Hence, $p^2 = M_\Phi^2$. The plotted ratio can be seen in Fig. 6a-c for a non-relativistic, slightly relativistic and highly relativistic incoming particle Φ. In the figures, the limiting case of $M_\Phi^2 \gg (m_1 + m_2)^2$ was used rendering the loop-particles effectively massless. With these simplifications, the figures reproduce the findings of Ho and Scherrer [28]. Their work considered the case of identical loop masses $m_1 = m_2 = 0$ evaluated in the imaginary-time formalism and their result has here been verified in the real-time formalism. The limit as $T \to 0$ is $R_{\Phi \to \phi\phi} \to 1$ as expected.

The deviation from [28] when loop masses m_1, m_2 are not identical was investigated. Such deviations are clearly relevant only in the case of $M_\Phi \sim m_1, m_2$, close to the equality of $M_\Phi^2 = (m_1 + m_2)^2$. An analysis of the self-energy presented earlier in this section shows that the behaviour is qualitatively similar to Fig. 6a-c also close to the equality. Further, in another mass region $0 \leq M_\Phi^2 < (m_1 - m_2)^2$ or for virtual particles Φ with $p^2 < 0$, the behaviour of $\Gamma_{\Phi \to \phi\phi}$ also here is quadratically growing with temperature. Hence, these regions do not differ in behaviour compared to the plotted cases.

4 Scalar decay into a fermion-antifermion pair

This section presents the thermal rate at which a neutral scalar particle Φ decays into a fermion-antifermion pair $\psi^2\bar{\psi}^1$. One model that gives rise to such decay process is

$$\mathcal{L}_{\text{int}} = a\Phi\bar{\psi}^1\psi^2. \tag{4.1}$$

The particles are associated with masses M for Φ and m_i for ψ^i.

4.1 The real-time self-energy of the fermion-antifermion eye-diagram

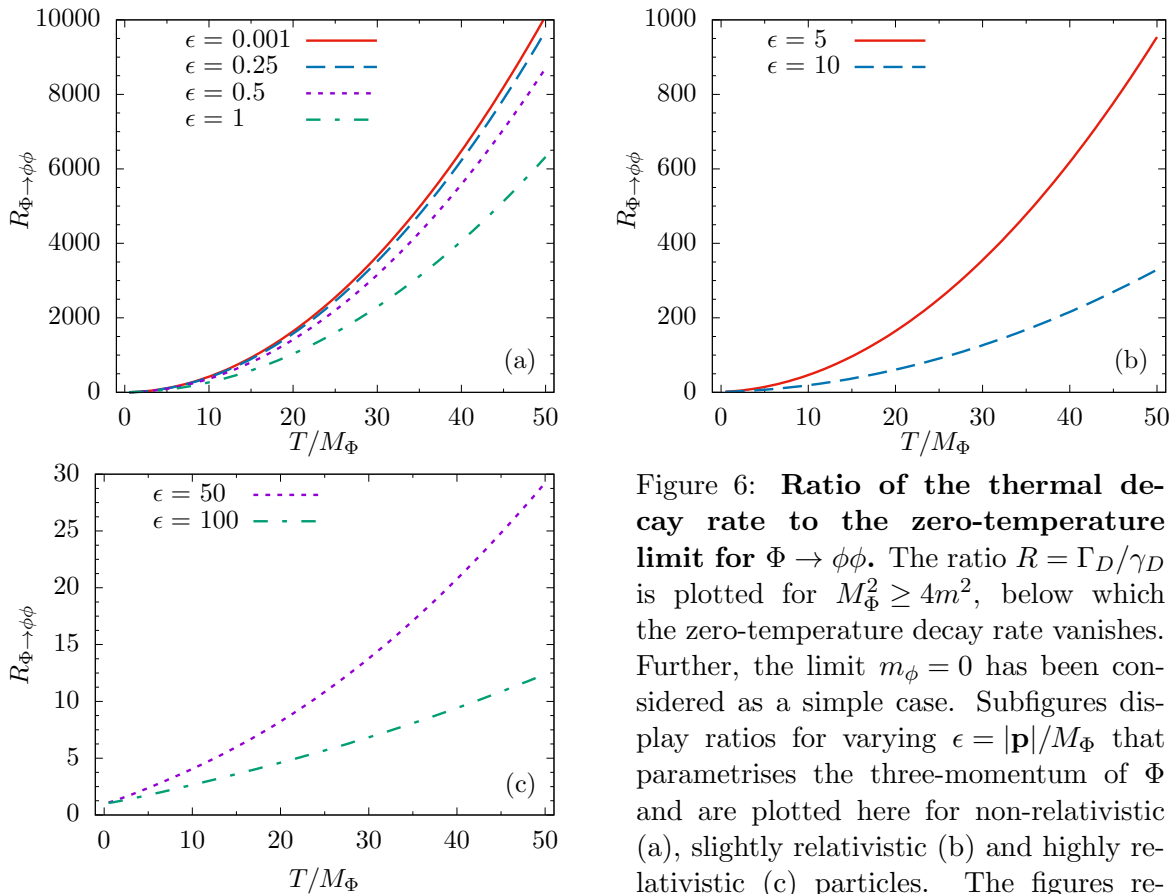Using the interaction term of Eq. (4.1), the following eye-diagram may be drawn:

$$\tag{4.2}$$

Figure 6: **Ratio of the thermal decay rate to the zero-temperature limit for $\Phi \to \phi\phi$.** The ratio $R = \Gamma_D/\gamma_D$ is plotted for $M_\Phi^2 \geq 4m^2$, below which the zero-temperature decay rate vanishes. Further, the limit $m_\phi = 0$ has been considered as a simple case. Subfigures display ratios for varying $\epsilon = |\mathbf{p}|/M_\Phi$ that parametrises the three-momentum of Φ and are plotted here for non-relativistic (a), slightly relativistic (b) and highly relativistic (c) particles. The figures reproduce the results of [28]. Note that $R \to 1$ when T vanishes.

The Φ-lines may connect to either external legs or vertices and will be amputated in the following calculation of the self-energy.

As in the case of the scalar-scalar loop of Sec. 3, the self-energy of this diagram is related to the thermal decay rate of the process $\Phi \to \psi^2\bar{\psi}^1$. The self-energy is defined as the bubble

$$i\mathcal{I}_{\text{bubble}}(p; m_1, m_2) = \quad\quad . \tag{4.3}$$

Also here, all valid combinations of field components must be taken into account, as has been indicated by the thick lines that represent the matrix propagator, but only one self-energy component is independent, see Eq. (2.114). The evaluation of the self-energy (++)-component

is sufficient to extract the thermal decay rate. This component is

$$
i\mathcal{I}_{\text{bubble}}^{(++)}(p; m_1, m_2)
$$

$$
= i(-ia)^2(-1) \int \frac{\mathrm{d}^4 k}{(2\pi)^4} \, \mathrm{tr}\left[i\tilde{S}_{\text{F}}^{(++)}(k-p; m_1) i\tilde{S}_{\text{F}}^{(++)}(k; m_2) \right]
$$

$$
= i(-ia)^2(-1) \int \frac{\mathrm{d}^4 k}{(2\pi)^4} \, \mathrm{tr}\left[-i\tilde{S}_{\bar{\text{F}}}^{(++)}(p-k; m_1) i\tilde{S}_{\text{F}}^{(++)}(k; m_2) \right]
$$

$$
= iI_{\text{F}\bar{\text{F}}}^{(2)}(p^2; m_1, m_2) + \left[iF_{\text{F}\bar{\text{F}}}^{(2)}(p; m_1, m_2) + (\text{F} \leftrightarrow \bar{\text{F}}) \right] + iF_{\text{F}\bar{\text{F}}}^{(3)}(p; m_1, m_2). \qquad (4.4)
$$

Note that an extra minus sign appears as well as the trace over spin space in the case of a fermion loop. The bracketed arrow represents the second mixed integral that arises from propagator cross terms. As in the case of the scalar-scalar loop, the bubble splits into four terms. The explicit integrals are

$$
iI_{\text{F}\bar{\text{F}}}^{(2)}(p^2; m_1, m_2)
$$

$$
= i(-ia)^2 \int \frac{\mathrm{d}^4 k}{(2\pi)^4} \, \mathrm{tr}\left[\frac{i\big((\not{p} - \not{k}) - m_1\big)}{(p-k)^2 - m_1^2 + i\epsilon} \frac{i\big(\not{k} + m_2\big)}{k^2 - m_2^2 + i\epsilon} \right], \qquad (4.5)
$$

$$
iF_{\text{F}\bar{\text{F}}}^{(2)}(p; m_1, m_2)
$$

$$
= i(-ia)^2 \int \frac{\mathrm{d}^4 k}{(2\pi)^4} \, \mathrm{tr}\left[\frac{i\big((\not{p} - \not{k}) - m_1\big)}{(p-k)^2 - m_1^2 + i\epsilon} (-2\pi)\big(\not{k} + m_2\big) n_{\text{F}}(k_0)\delta\big(k^2 - m_2^2\big) \right], \qquad (4.6)
$$

$$
iF_{\text{F}\bar{\text{F}}}^{(3)}(p; m_1, m_2)
$$

$$
= i(-ia)^2 \int \frac{\mathrm{d}^4 k}{(2\pi)^4} \, \mathrm{tr}\Big[(-2\pi)\big((\not{p} - \not{k}) - m_1\big) n_{\bar{\text{F}}}(p_0 - k_0)\delta\big((p-k)^2 - m_1^2\big) \times
$$

$$
\times (-2\pi)\big(\not{k} + m_2\big) n_{\text{F}}(k_0)\delta\big(k^2 - m_2^2\big) \Big]. \qquad (4.7)
$$

The trace is common to all integrals and evaluates to

$$
\mathrm{tr}\left[\big((\not{p} - \not{k}) - m_1\big)\big(\not{k} + m_2\big) \right] = -4\big(m_1 m_2 - p \cdot k + k^2\big). \qquad (4.8)
$$

4.1.1   The non-thermal self-energy term

The non-thermal contribution is again known from zero-temperature theory but the full integral is cumbersome to evaluate in comparison to the case of the scalar-scalar loop. However, by rewriting the logarithm resulting from dimensional regularisation according to

$$
\ln\big[x \pm i\epsilon\big] = \ln|x| \pm i\pi\Theta(x), \qquad (4.9)
$$

with $\Theta(x)$ being the Heaviside step-function, the imaginary part of interest to the decay rate calculation may be extracted. The imaginary part of $iI^{(2)}_{\mathrm{F\bar{F}}}(p^2; m_1, m_2)$ is

$$\Im\left[iI^{(2)}_{\mathrm{F\bar{F}}}(p^2; m_1, m_2)\right] = \frac{a^2}{8\pi}\sqrt{C}\times$$

$$\times\begin{cases} \dfrac{p^2}{2}\left[C - \left(1 + \dfrac{m_2^2 - m_1^2}{p^2}\right)^2\right] - p^2\left(1 + \dfrac{m_2^2 - m_1^2}{p^2}\right) + 2m_2\left[m_1 + 2m_2\right] & \text{if (a),} \\ 0 & \text{otherwise,} \end{cases} \tag{4.10}$$

where C is identical to the definition in Sec. 3. In the case of identical loop masses, the expression reduces to

$$\Im\left[iI^{(2)}_{\mathrm{F\bar{F}}}(p^2; m_1, m_2)\right] = \begin{cases} -\dfrac{a^2\left(p^2 - 4m^2\right)}{8\pi}\sqrt{1 - \dfrac{4m^2}{p^2}} & \text{if (a),} \\ 0 & \text{otherwise.} \end{cases} \tag{4.11}$$

This matches literature, e.g. [29].

4.1.2 The mixed self-energy term

The mixed self-energy contribution consists of two complex cross terms. The evaluation of the imaginary component of those terms results in

$$\Im\left[iF^{(2)}_{\mathrm{F\bar{F}}}(p; m_1, m_2) + (\mathrm{F} \leftrightarrow \mathrm{\bar{F}})\right] = -\frac{a^2}{8\pi|\mathbf{p}|\beta}\left(p^2 - (m_2 + m_1)^2\right)\times$$

$$\times\begin{cases} \ln\left[\dfrac{\left(e^{-\beta(\omega_{2,p_+}-\mu)} + 1\right)\left(e^{-\beta(\omega_{1,p_+}+\mu)} + 1\right)}{\left(e^{-\beta(\omega_{2,p_-}-\mu)} + 1\right)\left(e^{-\beta(\omega_{1,p_-}+\mu)} + 1\right)}\right] & \text{if (a) } \vee \left\{(\mathrm{c1}) \wedge m_2 \geq m_1\right\}, \\[3ex] 0 & \text{if (b),} \\[3ex] \ln\left[\dfrac{\left(e^{-\beta(\omega_{2,p_+}+\mu)} + 1\right)\left(e^{-\beta(\omega_{1,p_+}-\mu)} + 1\right)}{\left(e^{-\beta(\omega_{2,p_-}+\mu)} + 1\right)\left(e^{-\beta(\omega_{1,p_-}-\mu)} + 1\right)}\right] & \text{if (c1) } \wedge \ m_2 < m_1, \\[3ex] -\ln\left[\left(e^{-\beta(\omega_{2,p_+}-\mu)}+1\right)\left(e^{-\beta(\omega_{1,p_+}+\mu)}+1\right)\left(e^{-\beta(\omega_{2,p_-}-\mu)}+1\right)\left(e^{-\beta(\omega_{1,p_-}+\mu)}+1\right)\right] & \\ & \text{if (c2).} \end{cases}$$
$$\tag{4.12}$$

Here $\omega_{1,p_\pm}$ has been defined analogously to $\omega_{2,p_\pm}$ of Sec. 3 with interchanged masses.

In compact notation, the real part may be written as

$$\Re\left[iF_{\mathrm{F\bar{F}}}^{(2)}(p;m_1,m_2)+(\mathrm{F}\leftrightarrow\bar{\mathrm{F}})\right]$$

$$=\frac{a^2}{4\pi^2|\mathbf{p}|}\sum_{s=\pm}\times$$

$$\times\left\{\int_{m_2}^{\infty}\mathrm{d}\omega_{2,\mathbf{k}}\,n_{\mathrm{F},2}^{s}\left[C_2^s\mathcal{P}\ln\left|\frac{A_{21,+}^{(s)}}{A_{21,-}^{(s)}}\right|+\mathcal{P}\left(2|\mathbf{p}|\sqrt{\omega_{2,\mathbf{k}}^2-m_2^2}+D_{21}^s\ln\left|\frac{A_{21,-}^{(s)}}{A_{21,+}^{(s)}}\right|\right)\right]\right.$$

$$\left.+\int_{m_1}^{\infty}\mathrm{d}\omega_{1,\mathbf{k}}\,n_{\mathrm{F},1}^{-s}\left[C_1^s\mathcal{P}\ln\left|\frac{A_{12,+}^{(s)}}{A_{12,-}^{(s)}}\right|+\mathcal{P}\left(2|\mathbf{p}|\sqrt{\omega_{1,\mathbf{k}}^2-m_1^2}+D_{12}^s\ln\left|\frac{A_{12,-}^{(s)}}{A_{12,+}^{(s)}}\right|\right)\right]\right\},\quad(4.13)$$

where the following functions have been defined:

$$\omega_{1,\mathbf{k}}^2=|\mathbf{k}|^2+m_1^2,\tag{4.14}$$

$$n_{\eta,i}^{\pm}=\frac{1}{e^{\beta(\omega_{i,\mathbf{k}}\pm\mu)}-\eta},\qquad\eta=\pm1\text{ for bosons(B)/fermions(F)},\tag{4.15}$$

$$C_i^{\pm}=m_im_j\pm p_0\omega_{i,\mathbf{k}}+m_i^2,\tag{4.16}$$

$$D_{ij}^{\pm}=\frac{1}{2}\left(p^2\pm2p_0\omega_{i,\mathbf{k}}+m_i^2-m_j^2\right),\tag{4.17}$$

$$A_{ij,\pm}^{(\pm)}=p^2(\pm)2p_0\omega_{i,\mathbf{k}}\pm2|\mathbf{p}|\sqrt{\omega_{i,\mathbf{k}}^2-m_i^2}+m_i^2-m_j^2.\tag{4.18}$$

4.1.3 The purely thermal self-energy term

The purely thermal contribution to the self-energy has no real component and was found to be

$$iF_{\mathrm{F\bar{F}}}^{(3)}(p;m_1,m_2)=-i\frac{a^2}{4\pi|\mathbf{p}|\beta}\left(p^2-(m_1+m_2)^2\right)\times$$

$$\times\left\{\begin{array}{ll}\dfrac{1}{e^{\beta p_0}-1}\ln\left[\dfrac{\left(e^{-\beta(\omega_{2,p_+}-\mu)}+1\right)\left(e^{\beta(p_0-\omega_{2,p_-}+\mu)}+1\right)}{\left(e^{-\beta(\omega_{2,p_-}-\mu)}+1\right)\left(e^{\beta(p_0-\omega_{2,p_+}+\mu)}+1\right)}\right]&\text{if (a)},\\[2em]0&\text{if (b)},\\[1em]\dfrac{1}{e^{\mp\beta p_0}-1}\left\{e^{\mp\beta p_0}\ln\left[\dfrac{e^{-\beta(\omega_{2,p_+}\mp(p_0+\mu))}+1}{e^{-\beta(\omega_{2,p_-}\mp(p_0+\mu))}+1}\right]+\ln\left[\dfrac{e^{-\beta(\omega_{2,p_+}\mp\mu)}+1}{e^{-\beta(\omega_{2,p_-}\mp\mu)}+1}\right]\right\}&\text{if (c1) }\wedge\text{ (d1),}\\[2em]\dfrac{1}{e^{-\beta p_0}-1}\left\{e^{-\beta p_0}\ln\left[e^{-\beta(\omega_{2,p_\pm}-p_0-\mu)}+1\right]-\ln\left[e^{-\beta(\omega_{2,p_\pm}-\mu)}+1\right]\right\}\\[1em]\quad+\dfrac{1}{e^{\beta p_0}-1}\left\{e^{\beta p_0}\ln\left[e^{-\beta(\omega_{2,p_\mp}+p_0+\mu)}+1\right]-\ln\left[e^{-\beta(\omega_{2,p_\mp}+\mu)}+1\right]\right\}&\text{if (c2) }\wedge\text{ (d2).}\end{array}\right.\tag{4.19}$$

Note that in this final expression for the purely thermal contribution, the mass parameters m_1, m_2 should again be replaced by $\min\{m_1,m_2\}$ and $\max\{m_1,m_2\}$ respectively; cf. Sec. 3.1.3.

The $(++)$-component of the self-energy of the fermionic eye-diagram presented in Sec. 4.1.1-4.1.3 has not been found in the literature.

4.1.4 Decay rate of $\Phi \to \psi^2 \bar{\psi}^1$

The thermal decay rate of a neutral scalar is given by Eq. (2.125) in Sec. 2.7.2. In the special case of the two loop masses being identical, the expression for the self-energy is reduced significantly due to the simplification of the factors C and $\omega_{i,p_\pm}$. The ratio of Eq. (2.127) may be obtained in the mass region of $M_\Phi^2 \geq (m_1 + m_2)^2$ were the zero-temperature decay rate is non-vanishing. Φ is simply put on-shell so that $p^2 = M_\Phi^2$. The plotted ratio can be seen for non-relativistic, slightly relativistic and highly relativistic Φ in Fig. 7 taking the simplification $m_1 = m_2 = 0$ as a limiting case. Then, the figure reproduces the findings of Ho and Scherrer [28] who evaluated the loop in the imaginary-time formalism. Their result was reproduced here in the real-time formalism. The limit as $T \to 0$ is $R_{\Phi \to \psi\bar{\psi}} \to 1$, shown in Fig. 8.
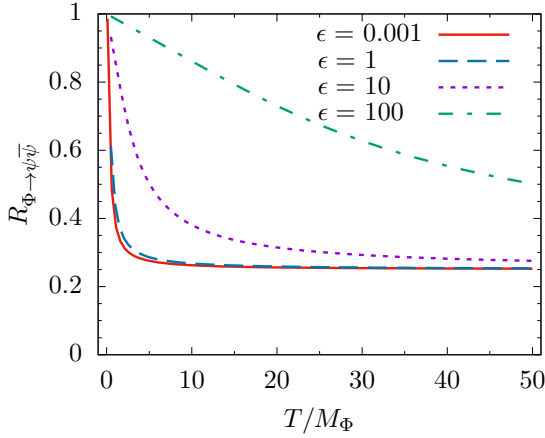
Figure 7: **Ratio of the thermal decay rate to the zero-temperature limit for $\Phi \to \psi\bar{\psi}$.** The ratio $R = \Gamma_D/\gamma_D$ is plotted for $M_\Phi^2 \geq 4m_\psi^2$ below which the zero-temperature quantity vanishes. Further, $m_\psi = 0$ was used for simplification. Varying $\epsilon = |\mathbf{p}|/M_\Phi$, a parametrisation of the three momentum of Φ, ratios are plotted for a non-relativistic (solid and dashed), slightly relativistic (dotted) and highly relativistic (dash-dotted) particle Φ. The figure reproduces the result of [28].
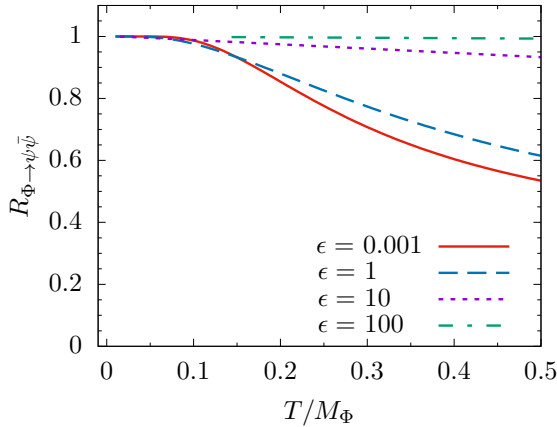

Figure 8: **Ratio of the thermal decay rate to the zero-temperature limit for $\Phi \to \psi\bar{\psi}$.** The ratio $R = \Gamma_D/\gamma_D$ is plotted for $M_\Phi^2 \geq m_\psi^2$, below which the zero-temperature quantity vanishes, in the region of low temperature. Further, $m_\psi = 0$ is used as a simple case. Varying $\epsilon = |\mathbf{p}|/M_\Phi$, a parametrisation of the three momentum of Φ, ratios are plotted for a non-relativistic (solid and dashed), slightly relativistic (dotted) and highly relativistic (dash-dotted) particle Φ.

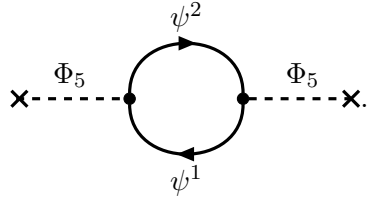# 5 Pseudoscalar decay into a fermion-antifermion pair

This section presents the thermal rate at which a neutral pseudoscalar particle Φ_5 decays into a fermion-antifermion pair $\psi^2\bar{\psi}^1$ as calculated in this thesis work. One model giving rise to such a process is

$$\mathcal{L}_{\text{int}} = b\Phi_5\bar{\psi}^1\gamma_5\psi^2. \tag{5.1}$$

The vertex factor of γ_5 naïvely requires some care when computing the decay of Φ_5 into a fermion-antifermion pair through the fermionic loop in contrast to the scalar-scalar loop considered in Sec. 3 that has no spinor structure. Masses have been assigned according to M for Φ_5 and m_i for ψ^i.

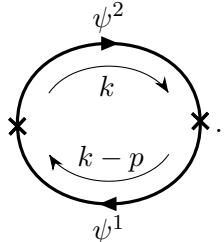## 5.1 The real-time self-energy of the fermion-antifermion eye-diagram

Using the interaction term of Eq. (5.1), the following eye-diagram may be drawn:

$$\tag{5.2}$$

The Φ_5-lines connect either to external legs or vertices and will be amputated in the following calculation of the self-energy.

As in the case of the scalar-scalar loop of Sec. 3, the self-energy of this diagram is related to the thermal decay rate (see Eq. (2.125)). The self-energy is defined as the bubble

$$i\mathcal{I}_{\text{bubble}}(p;m_1,m_2) = \tag{5.3}$$

Again, all valid combinations of propagators must be taken into account but only one component of the self-energy is independent, see Eq. (2.114), and the evaluation of the $(++)$-component is sufficient in order to extract the thermal decay rate. Note that the bubble above is very similar to the case of an external *scalar* that was considered in Sec. 4. The discrepancy is one insertion of γ_5 at each vertex and this factor does not trivially commute with the fermion propagator. The $(++)$-component is

$$i\mathcal{I}_{\text{bubble}}^{(++)}(p;m_1,m_2)$$

$$= i(-ib)^2(-1)\int\frac{\mathrm{d}^4k}{(2\pi)^4}\,\mathrm{tr}\Big[\gamma_5 i\tilde{S}_{\text{F}}^{(++)}(k-p;m_1)\gamma_5 i\tilde{S}_{\text{F}}^{(++)}(k;m_2)\Big]$$

$$= i(-ib)^2(-1)\int\frac{\mathrm{d}^4k}{(2\pi)^4}\,\mathrm{tr}\Big[-\gamma_5 i\tilde{S}_{\bar{\text{F}}}^{(++)}(p-k;m_1)\gamma_5 i\tilde{S}_{\text{F}}^{(++)}(k;m_2)\Big]$$

$$= iI_{\text{F}\bar{\text{F}}}^{(4)}(p^2;m_1,m_2) + \Big[iF_{\text{F}\bar{\text{F}}}^{(4)}(p;m_1,m_2) + (\text{F}\leftrightarrow\bar{\text{F}})\Big] + iF_{\text{F}\bar{\text{F}}}^{(5)}(p;m_1,m_2). \tag{5.4}$$

As for the $\Phi \to \psi^2\bar{\psi}^1$-process considered in the previous section, an overall minus sign appears as well as the trace over γ-matrices. The bubble splits into four terms and the bracketed arrow denotes the second mixed cross term. The explicit integrals are

$$iI_{\mathrm{F\bar{F}}}^{(4)}(p^2;m_1,m_2)$$
$$= i(-ib)^2\!\int\frac{\mathrm{d}^4k}{(2\pi)^4}\ \mathrm{tr}\!\left[\gamma_5\frac{i\big((\slashed{p}-\slashed{k})-m_1\big)}{(p-k)^2-m_1^2+i\epsilon}\gamma_5\frac{i\big(\slashed{k}+m_2\big)}{k^2-m_2^2+i\epsilon}\right],\tag{5.5}$$

$$iF_{\mathrm{F\bar{F}}}^{(4)}(p;m_1,m_2)$$
$$= i(-ib)^2\!\int\frac{\mathrm{d}^4k}{(2\pi)^4}\ \mathrm{tr}\!\left[\gamma_5\frac{i\big((\slashed{p}-\slashed{k})-m_1\big)}{(p-k)^2-m_1^2+i\epsilon}\gamma_5(-2\pi)\big(\slashed{k}+m_2\big)n_{\mathrm{F}}(k_0)\delta\big(k^2-m_2^2\big)\right],\tag{5.6}$$

$$iF_{\mathrm{F\bar{F}}}^{(5)}(p;m_1,m_2)$$
$$= i(-ib)^2\!\int\frac{\mathrm{d}^4k}{(2\pi)^4}\ \mathrm{tr}\Big[\gamma_5(-2\pi)\big((\slashed{p}-\slashed{k})-m_1\big)n_{\bar{\mathrm{F}}}(p_0-k_0)\delta\big((p-k)^2-m_1^2\big)\times$$
$$\times\ \gamma_5(-2\pi)\big(\slashed{k}+m_2\big)n_{\mathrm{F}}(k_0)\delta\big(k^2-m_2^2\big)\Big].\tag{5.7}$$

The trace may be performed in the naïve dimensional regularisation scheme since the diagram appears at one-loop level.[16] See [30] for a condensed but comprehensive and general discussion on γ-matrices and γ_5 in D-dimensional schemes. The trace evaluated in the naïve dimensional regularisation scheme is

$$\mathrm{tr}\left[\gamma_5\big((\slashed{p}-\slashed{k})-m_1\big)\gamma_5\big(\slashed{k}+m_2\big)\right] = 4\big(-m_1m_2-p\cdot k+k^2\big).\tag{5.8}$$

The sign differences compared to the case of a decaying *scalar* particle are an overall positive sign together with the minus sign in front of m_1m_2. The overall sign change may be reverted by imposing hermiticity of the Lagrangian and thereby force the pseudoscalar coupling to $\bar{\psi}^1\gamma_5\psi^2$ to become purely imaginary, i.e. $b=i|b|$. The apparent negative mass, of either m_1 or m_2, is more intriguing and signifies a fundamental difference between the scalar and pseudoscalar decay rates.[17]

Apart from the mentioned differences in relative signs, the resulting self-energy integrals for the pseudoscalar case are identical to those for the scalar case. To obtain the correct non-thermal, mixed and purely thermal self-energy integrals it is sufficient to change the overall sign in the scalar results as well as to replace $m_1 \to -m_1$.

5.1.1 The non-thermal self-energy term

The non-thermal contribution in the case of an external pseudoscalar particle is related to the case of an external *scalar* particle as

$$iI_{\mathrm{F\bar{F}}}^{(4)}\big(p^2;m_1,m_2\big) = -\,iI_{\mathrm{F\bar{F}}}^{(2)}\big(p^2;-m_1,m_2\big).\tag{5.9}$$

---

[16]Calculations could potentially require a more robust technique at higher loop orders. For example in the evaluation of 3-body decays another scheme is required. [30]

[17]Note that the wording "negative mass" is purely a heuristic, here denoting the relative sign difference between the scalar and pseudoscalar results.

The right-hand side is the result of Sec. 4.1.1.

5.1.2 The mixed self-energy term

The mixed thermal contribution in the case of an external pseudoscalar particle is related to the case of an external *scalar* particle as

$$\Im\left[iF_{\text{F}\bar{\text{F}}}^{(4)}(p;m_1,m_2)+(\text{F}\leftrightarrow\bar{\text{F}})\right]=-\Im\left[iF_{\text{F}\bar{\text{F}}}^{(2)}(p;-m_1,m_2)+(\text{F}\leftrightarrow\bar{\text{F}})\right] \tag{5.10}$$

and

$$\Re\left[iF_{\text{F}\bar{\text{F}}}^{(4)}(p;m_1,m_2)+(\text{F}\leftrightarrow\bar{\text{F}})\right]=-\Re\left[iF_{\text{F}\bar{\text{F}}}^{(2)}(p;-m_1,m_2)+(\text{F}\leftrightarrow\bar{\text{F}})\right]. \tag{5.11}$$

The right-hand side is the result of Sec. 4.1.2.

5.1.3 The purely thermal self-energy term

The purely thermal contribution in the case of an external pseudoscalar particle is related to the case of an external *scalar* particle as

$$iF_{\text{F}\bar{\text{F}}}^{(5)}(p;m_1,m_2)=-iF_{\text{F}\bar{\text{F}}}^{(3)}(p;-m_1,m_2) \tag{5.12}$$

The right-hand side is the result of Sec. 4.1.3.

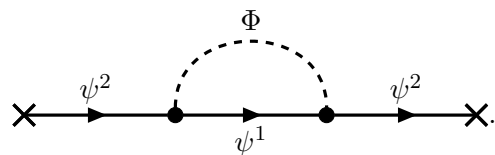### 5.1.4 Decay rate of $\Phi_5\to\psi^2\bar{\psi}^1$

The thermal decay rate of a neutral pseudoscalar is given by Eq. (2.125) in Sec. 2.7.2. The resulting expression is similar to the case of a decaying scalar. The sign change preceding one of the loop masses enhances the decay rate for the pseudoscalar relative to the scalar decay rate in the region of $M_\Phi^2\sim(m_1+m_2)^2$ where Φ has been put on-shell ($p^2=M_\Phi^2$). Taking $m_1=m_2=m$ and normalising M_Φ in units of m, the ratio $\Gamma_{\Phi_5\to\psi\bar{\psi}}/\Gamma_{\Phi\to\psi\bar{\psi}}$ as a function of the mass of the external (pseudo)scalar is shown in Fig. 9 for this momentum region. Close to the equality $M_\Phi^2=4m^2$, the expression diverges which implies that the scalar decay rate vanishes quicker than the pseudoscalar decay rate. Normalising the fermion mass to $m=1$, the ratio diverges at 2. This is a non-thermal effect, independent of temperature.

6 Emission of a (pseudo)scalar off a fermion

The interaction term of Eq. (4.1) in Sec. 4 allows for the emission of a scalar off a fermion line. The amplitude for such emission may be evaluated by considering (pseudo)scalar corrections to the fermion line. In this section, the thermal self-energy of the scalar-fermion one-loop diagram is presented.

6.1 The real-time self-energy of the scalar-fermion eye-diagram

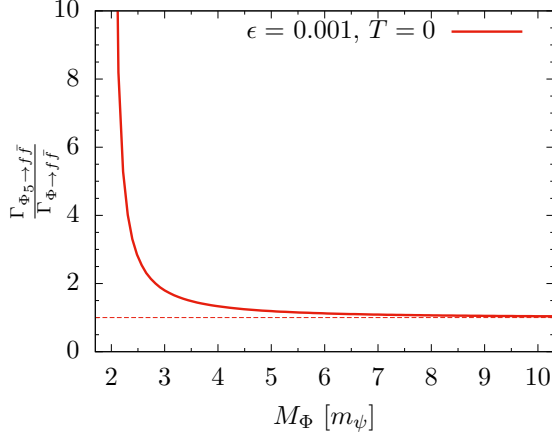The scalar-fermion interaction term of Eq. (4.1) gives rise to the eye-diagram

$$\tag{6.1}$$

Figure 9: **Ratio of the pseudo-scalar decay rate to the scalar ditto.** The ratio $\Gamma_{\Phi_5 \to \psi\bar\psi}/\Gamma_{\Phi \to \psi\bar\psi}$ is plotted for $M_\Phi^2 \geq 4m_\psi^2$, fermion masses in the loop being equal, as a function of the mass of the decaying scalar. Here $M_\Phi = M_{\Phi_5}$ for comparison and expressed in terms of m_ψ. The pseudoscalar decay rate is enhanced relative to the scalar quantity close to the equality $M_\Phi^2 = 4m_\psi^2$. This behaviour was verified for a broad range of both $\epsilon = |\mathbf{p}|/M_\Phi \in [0.001, 100]$ and $T/M_\Phi \in [0, 1000]$.

As in previous sections, the thick lines of the loop denote the full real-time thermal propagator in its matrix structure with components of Eqs. 2.95, 2.100. The ψ^2-lines may connect either to vertices or external legs. This diagram in itself is on matrix form and represents the full sum of thermal diagrams, similar to the case of the scalar bubble in Sec. 3, including both physical chronological and unphysical antichronological field components. Using the convention as for previous calculations, the self-energy matrix is defined as the bubble

$$i\mathcal{I}_{\text{bubble}}(p; m_1, M) = \quad (6.2)$$

where, for the case of interest, vertices couple to fermion lines on external legs. The $(++)$-component of this bubble is

$$i\mathcal{I}_{\text{bubble}}^{(++)}(p; m_1, M)$$
$$= i(-ia)^2 \int \frac{\mathrm{d}^4 k}{(2\pi)^4} \, i\tilde{S}_{\text{F}}^{(++)}(p - k; m_1) i\tilde{D}^{(++)}(-k; M)]$$
$$= iI_{\text{SF}}^{(2)}(p; m_1, M) + \left[iF_{\text{SF}}^{(2)}(p; m_1, M) + (\text{S} \leftrightarrow \text{F}) \right] + iF_{\text{SF}}^{(3)}(p; m_1, M). \quad (6.3)$$

The four integrals extracted above are the non-thermal contribution, the mixed thermal contribution and the purely thermal contribution to the loop. The second mixed term, expressed through the bracketed arrow, is similar to its preceding term but with the thermal term of the fermion propagator and the non-thermal term of the boson propagator interchanged. The

explicit forms are

$$
\begin{aligned}
&iI_{\text{SF}}^{(2)}(p; m_1, M) \\
&\quad = i(-ia)^2 \int \frac{\mathrm{d}^4 k}{(2\pi)^4} \frac{i\big((\not{p} - \not{k}) + m_1\big)}{(p-k)^2 - m_1^2 + i\epsilon} \frac{i}{k^2 - M^2 + i\epsilon},
\end{aligned}
\tag{6.4}
$$

$$
\begin{aligned}
&iF_{\text{SF}}^{(2)}(p; m_1, M) \\
&\quad = i(-ia)^2 \int \frac{\mathrm{d}^4 k}{(2\pi)^4} \frac{i\big((\not{p} - \not{k}) + m_1\big)}{(p-k)^2 - m_1^2 + i\epsilon} 2\pi\, n_{\text{B}}(|k_0|)\delta\big(k^2 - M^2\big),
\end{aligned}
\tag{6.5}
$$

$$
\begin{aligned}
&(\text{S} \leftrightarrow \text{F}) \\
&\quad = i(-ia)^2 \int \frac{\mathrm{d}^4 k}{(2\pi)^4} (-2\pi)\big((\not{p}-\not{k}) + m_1\big)\, n_{\text{F}}(p_0 - k_0)\delta\big((p-k)^2 - m_1^2\big)\frac{i}{k^2 - M^2 + i\epsilon},
\end{aligned}
\tag{6.6}
$$

$$
\begin{aligned}
&iF_{\text{SF}}^{(3)}(p; m_1, M) \\
&\quad = i(-ia)^2 \int \frac{\mathrm{d}^4 k}{(2\pi)^4} (-2\pi)\big((\not{p} - \not{k}) + m_1\big)n_{\text{F}}(p_0 - k_0)\delta\big((p-k)^2 - m_1^2\big) \times \\
&\qquad\qquad \times\, 2\pi n_{\text{B}}(|k_0|)\delta\big(k^2 - M^2\big).
\end{aligned}
\tag{6.7}
$$

6.1.1   The non-thermal self-energy term

Relevant to the emission is the imaginary part of the non-thermal contribution to the $(++)$-component of the self-energy. It may be extracted by a similar procedure performed in Sec. 4.1.1. Evaluated by dimensional regularisation techniques, the imaginary part of Eq. (6.4) is

$$
\Im\big[iI_{\text{SF}}^{(2)}(p; m_1, M)\big] = -\frac{a^2}{32\pi}\sqrt{C'} \times
\begin{cases}
\not{p}\Big(1 + \dfrac{m_1^2 - M^2}{p^2}\Big) + 2m_1 & \text{if } p^2 \geq (m_1 + M)^2, \\
0 & \text{otherwise.}
\end{cases}
\tag{6.8}
$$

Here

$$
C' = \Big(1 - \frac{(m_1 + M)^2}{p^2}\Big)\Big(1 - \frac{(m_1 - M)^2}{p^2}\Big).
\tag{6.9}
$$

6.1.2   The mixed self-energy term

The mixed self-energy contribution consists of two complex cross terms from the product of the propagators: the integrals in Eqs. (6.5) and (6.6). The resulting imaginary component of the sum of the integrals is a rather long expression when written down explicitly. For clarity, the result is therefore presented for each momentum region separately.

If $p^2 \geq (m_1 + M)^2$:

$$\Im\left[iF_{\mathrm{SF}}^{(2)}(p; m_1, M) + (\mathrm{S} \leftrightarrow \mathrm{F})\right]$$

$$= -\frac{a^2}{16\pi|\mathbf{p}|\beta}\left(\not{p} + \gamma^3\frac{-p^2+m_1^2-M^2}{2|\mathbf{p}|} + m_1\right)\ln\left|\frac{\left(e^{-\beta\omega_{M,p_+}}-1\right)\left(e^{\beta(\omega_{M,p_-}-p_0+\mu)}+1\right)}{\left(e^{-\beta\omega_{M,p_-}}-1\right)\left(e^{\beta(\omega_{M,p_+}-p_0+\mu)}+1\right)}\right|$$

$$- \frac{a^2}{16\pi|\mathbf{p}|\beta^2}\left(-\gamma^0 + \gamma^3\frac{p_0}{|\mathbf{p}|}\right) \times \left\{-\frac{\beta^2}{2}\left(\omega_{M,p_+}^2 - \omega_{M,p_-}^2\right)\right.$$

$$+ \mathrm{Li}_2\left(e^{\beta\omega_{M,p_+}}\right) - \mathrm{Li}_2\left(e^{\beta\omega_{M,p_-}}\right) - \mathrm{Li}_2\left(-e^{\beta(\omega_{M,p_+}-p_0+\mu)}\right) + \mathrm{Li}_2\left(-e^{\beta(\omega_{M,p_-}-p_0+\mu)}\right)$$

$$\left.+ \beta\omega_{M,p_+}\ln\left[\frac{1-e^{\beta\omega_{M,p_+}}}{e^{\beta(\omega_{M,p_+}-p_0+\mu)}+1}\right] - \beta\omega_{M,p_-}\ln\left[\frac{1-e^{\beta\omega_{M,p_-}}}{e^{\beta(\omega_{M,p_-}-p_0+\mu)}+1}\right]\right\}, \qquad (6.10)$$

where

$$\omega_{M,p_\pm} = \frac{1}{2}\left|p_0\left|1 + \frac{M^2-m_1^2}{p^2}\right| \pm |\mathbf{p}|\sqrt{C'}\right|. \qquad (6.11)$$

Further, $\mathrm{Li}_2(z)$ is the analytic continuation of Spence's function, the dilogarithm

$$\hat{\mathrm{Li}}_2(z) = -\int_0^z \mathrm{d}\tau\frac{\ln[1-\tau]}{\tau}, \quad z \in \mathbb{C}, \qquad (6.12)$$

which cancels exactly the imaginary part that arises from the negative sign of $1-e^{\beta\omega_{M,p_\pm}}$ in the two analytically continued logarithmic terms in Eq. (6.10).

If $(m_1 - M)^2 \leq p^2 < (m_1 + M)^2$:

$$\Im\left[iF_{\mathrm{SF}}^{(2)}(p; m_1, M) + (\mathrm{S} \leftrightarrow \mathrm{F})\right] = 0. \qquad (6.13)$$

If $0 \leq p^2 < (m_1 - M)^2$:

$$\Im\left[iF_{\mathrm{SF}}^{(2)}(p; m_1, M) + (\mathrm{S} \leftrightarrow \mathrm{F})\right]$$

$$= -\frac{a^2}{16\pi|\mathbf{p}|\beta}\left(\not{p} + \gamma^3\frac{-p^2+m_1^2-M^2}{2|\mathbf{p}|} + m_1\right)\ln\left|\frac{\left(e^{-\beta\omega_{M,p_+}}-1\right)\left(e^{\beta(\omega_{M,p_-}\mp(p_0-\mu))}+1\right)}{\left(e^{-\beta\omega_{M,p_-}}-1\right)\left(e^{\beta(\omega_{M,p_+}\mp(p_0-\mu))}+1\right)}\right|$$

$$\mp \frac{a^2}{16\pi|\mathbf{p}|\beta^2}\left(-\gamma^0 + \gamma^3\frac{p_0}{|\mathbf{p}|}\right) \times$$

$$\times\left\{\mathrm{Li}_2\left(e^{\beta\omega_{M,p_+}}\right) - \mathrm{Li}_2\left(e^{\beta\omega_{M,p_-}}\right) + \mathrm{Li}_2\left(-e^{\beta(\omega_{M,p_+}\mp(p_0-\mu))}\right) - \mathrm{Li}_2\left(-e^{\beta(\omega_{M,p_-}\mp(p_0+\mu))}\right)\right.$$

$$+ \beta\omega_{M,p_+}\ln\left[\left(e^{-\beta\omega_{M,p_+}}-1\right)\left(e^{\beta(\omega_{M,p_+}\mp(p_0-\mu))}+1\right)\right]$$

$$\left.- \beta\omega_{M,p_-}\ln\left[\left(e^{-\beta\omega_{M,p_-}}-1\right)\left(e^{\beta(\omega_{M,p_-}\mp(p_0-\mu))}+1\right)\right]\right\}. \qquad (6.14)$$

Here, the upper sign applies if $M \geq m_1$ and the lower sign if $M < m_1$. Compare to the similar case (d1) in Sec. 3.1.3.

If $p^2 < 0$:

$$\Im\left[iF_{\mathrm{SF}}^{(2)}(p;m_1,M) + (\mathrm{S}\leftrightarrow\mathrm{F})\right]$$

$$= +\frac{a^2}{16\pi|\mathbf{p}|\beta}\left(\not{p} + \gamma^3\frac{-p^2+m_1^2-M^2}{2|\mathbf{p}|} + m_1\right)\times$$

$$\times\ln\left|\left(e^{-\beta\omega_{M,p_\pm}}-1\right)\left(e^{-\beta\omega_{M,p_\mp}}-1\right)\left(e^{-\beta(\omega_{M,p_\pm}-p_0+\mu)}+1\right)\left(e^{-\beta(\omega_{M,p_\mp}+p_0-\mu)}+1\right)\right|$$

$$+\frac{a^2}{16\pi|\mathbf{p}|\beta^2}\left(-\gamma^0+\gamma^3\frac{p_0}{|\mathbf{p}|}\right)\times$$

$$\times\Bigg\{\mathrm{Li}_2\left(e^{\beta\omega_{M,p_\pm}}\right)-\mathrm{Li}_2\left(e^{\beta\omega_{M,p_\mp}}\right)+\mathrm{Li}_2\left(-e^{\beta(\omega_{M,p_\pm}-p_0+\mu)}\right)-\mathrm{Li}_2\left(-e^{\beta(\omega_{M,p_\mp}+p_0-\mu)}\right)$$

$$+\beta\omega_{M,p_\pm}\ln\left[\left(e^{-\beta\omega_{M,p_\pm}}-1\right)\left(e^{\beta(\omega_{M,p_\pm}-p_0+\mu)}+1\right)\right]$$

$$-\beta\omega_{M,p_\mp}\ln\left[\left(e^{-\beta\omega_{M,p_\mp}}-1\right)\left(e^{\beta(\omega_{M,p_\mp}+p_0-\mu)}+1\right)\right]\Bigg\}. \tag{6.15}$$

Here, the upper and lower signs correspond to the modified case (d2) defined in Sec. 3.1.3. The modification is analogous to the modification of the case (d1) in the section above for $0 \leq p^2 < (m_1 - M)^2$ and, as a consequence, the result depends on the mass hierarchy of M, m_1.

6.1.3 The purely thermal self-energy term

The purely thermal self-energy contribution in Eq. (6.7) is purely imaginary, cf. previous self-energy evaluations in Secs. 3.1.3, 4.1.3 and 5.1.3. The resulting expression for this term, after momentum integration, is again rather long. Therefore, different regions of p^2 are presented separately below for clarity.

If $p^2 \geq (m_1 + M)^2$:

$$iF_{\mathrm{SF}}^{(3)}(p;m_1,M)$$

$$= i\frac{a^2}{8\pi|\mathbf{p}|\beta}\left(\not{p} + \gamma^3\frac{-p^2+m_1^2-M^2}{2|\mathbf{p}|} + m_1\right)\frac{1}{e^{\beta(p_0-\mu)}+1}\ln\left|\frac{\left(1-e^{-\beta\omega_{M,p_+}}\right)\left(e^{\beta(p_0-\omega_{M,p_-}-\mu)}+1\right)}{\left(1-e^{-\beta\omega_{M,p_-}}\right)\left(e^{\beta(p_0-\omega_{M,p_+}-\mu)}+1\right)}\right|$$

$$+i\frac{a^2}{8\pi|\mathbf{p}|\beta^2}\left(\gamma^0-\gamma^3\frac{p_0}{|\mathbf{p}|}\right)\frac{1}{e^{\beta(p_0-\mu)}+1}\times$$

$$\times\Bigg\{\mathrm{Li}_2\left(e^{\beta\omega_{M,p_+}}\right)-\mathrm{Li}_2\left(e^{\beta\omega_{M,p_-}}\right)-\mathrm{Li}_2\left(-e^{\beta(\omega_{M,p_+}-p_0+\mu)}\right)+\mathrm{Li}_2\left(-e^{\beta(\omega_{M,p_-}-p_0+\mu)}\right)$$

$$+\beta\omega_{M,p_+}\ln\left[\frac{1-e^{\beta\omega_{M,p_+}}}{1+e^{\beta(\omega_{M,p_+}-p_0+\mu)}}\right]-\beta\omega_{M,p_-}\ln\left[\frac{1-e^{\beta\omega_{M,p_-}}}{1+e^{\beta(\omega_{M,p_-}-p_0+\mu)}}\right]\Bigg\}. \tag{6.16}$$

If $(m_1 - M)^2 \leq p^2 < (m_1 + M)^2$:

$$iF_{\mathrm{SF}}^{(3)}(p;m_1,M) = 0. \tag{6.17}$$

If $0 \leq p^2 < (m_1 - M)^2$**:**

$$iF_{\text{SF}}^{(3)}(p; m_1, M)$$

$$= i\frac{a^2}{8\pi|\mathbf{p}|\beta}\left(\not{p} + \gamma^3\frac{-p^2+m_1^2-M^2}{2|\mathbf{p}|} + m_1\right)\frac{1}{e^{\mp\beta(p_0-\mu)}+1} \times$$

$$\times\left[\ln\left|\frac{\left(1-e^{-\beta\omega_{M,p_+}}\right)}{\left(1-e^{-\beta\omega_{M,p_-}}\right)}\right| + e^{\mp\beta(p_0-\mu)}\ln\left|\frac{\left(e^{-\beta(\omega_{M,p_+}\mp(p_0-\mu))}+1\right)}{\left(e^{-\beta(\omega_{M,p_-}\mp(p_0-\mu))}+1\right)}\right|\right]$$

$$\mp i\frac{a^2}{8\pi|\mathbf{p}|\beta^2}\left(\gamma^0 - \gamma^3\frac{p_0}{|\mathbf{p}|}\right)\frac{1}{e^{\mp\beta(p_0-\mu)}+1} \times$$

$$\times\Bigg\{\left(e^{\mp\beta(p_0-\mu)}+1\right)\frac{\beta^2}{2}\left(\omega_{M,p_-}^2 - \omega_{M,p_+}^2\right) + \beta\omega_{M,p_+}\ln\left[1-e^{\beta\omega_{M,p_+}}\right] - \beta\omega_{M,p_-}\ln\left[1-e^{\beta\omega_{M,p_-}}\right]$$

$$+ e^{\mp\beta(p_0-\mu)}\left[\beta\omega_{M,p_+}\ln\left[e^{\beta(\omega_{M,p_+}\mp(p_0-\mu))}+1\right] - \beta\omega_{M,p_-}\ln\left[e^{\beta(\omega_{M,p_-}\mp(p_0-\mu))}+1\right]\right]$$

$$+ \text{Li}_2\left(e^{\beta\omega_{M,p_+}}\right) - \text{Li}_2\left(e^{\beta\omega_{M,p_-}}\right)$$

$$+ e^{\mp\beta(p_0-\mu)}\left[\text{Li}_2\left(-e^{\beta(\omega_{M,p_+}\mp(p_0-\mu))}\right) - \text{Li}_2\left(-e^{\beta(\omega_{M,p_-}\mp(p_0-\mu))}\right)\right]\Bigg\}. \tag{6.18}$$

Again, the upper and lower signs correspond to the modified case (d1) discussed in Sec. 6.1.2 in order to take into account the hierarchy of M, m_1.

If $p^2 < 0$**:**

$$iF_{\text{SF}}^{(3)}(p; m_1, M)$$

$$= -i\frac{a^2}{8\pi|\mathbf{p}|\beta}\left(\not{p} + \gamma^3\frac{-p^2+m_1^2-M^2}{2|\mathbf{p}|} + m_1\right) \times$$

$$\times\Bigg\{\frac{1}{e^{-\beta(p_0-\mu)}+1}\left[\ln\left|\left(e^{-\beta\omega_{M,p_\pm}}-1\right)\right| + e^{-\beta(p_0-\mu)}\ln\left|\left(e^{-\beta(\omega_{M,p_\pm}-p_0+\mu)}+1\right)\right|\right]$$

$$+ \frac{1}{e^{\beta(p_0-\mu)}+1}\left[\ln\left|\left(e^{-\beta\omega_{M,p_\mp}}-1\right)\right| + e^{\beta(p_0-\mu)}\ln\left|\left(e^{-\beta(\omega_{M,p_\mp}+p_0-\mu)}+1\right)\right|\right]\Bigg\}$$

$$- i\frac{a^2}{8\pi|\mathbf{p}|\beta^2}\left(-\gamma^0 + \gamma^3\frac{p_0}{|\mathbf{p}|}\right)\frac{1}{e^{-\beta(p_0-\mu)}+1} \times$$

$$\times\Bigg\{-\frac{\pi^2}{3} + \frac{\pi^2}{6}e^{-\beta(p_0-\mu)} + \frac{\beta^2}{2}(p_0-\mu)^2 e^{-\beta(p_0-\mu)} - \frac{1}{2}\left(1+e^{-\beta(p_0-\mu)}\right)\beta^2\omega_{M,p_\pm}^2$$

$$+ \beta\omega_{M,p_\pm}\left[\ln\left[1-e^{\beta\omega_{M,p_\pm}}\right] + e^{-\beta(p_0-\mu)}\ln\left|e^{\beta(\omega_{M,p_\pm}-p_0+\mu)}+1\right|\right]$$

$$+ \text{Li}_2\left(e^{\beta\omega_{M,p_\pm}}\right) + e^{-\beta(p_0-\mu)}\text{Li}_2\left(-e^{\beta(\omega_{M,p_\pm}-p_0+\mu)}\right)\Bigg\}$$

$$
-i\frac{a^2}{8\pi|\mathbf{p}|\beta^2}\left(-\gamma^0 + \gamma^3\frac{p_0}{|\mathbf{p}|}\right)\frac{1}{e^{\beta(p_0-\mu)}+1}\times
$$

$$
\times\left\{-\frac{\pi^2}{3} + \frac{\pi^2}{6}e^{\beta(p_0-\mu)} + \frac{\beta^2}{2}(p_0-\mu)^2 e^{\beta(p_0-\mu)} - \frac{1}{2}\left(1+e^{\beta(p_0-\mu)}\right)\beta^2\omega_{M,p_\mp}^2\right.
$$

$$
+ \beta\omega_{M,p_\mp}\left[\ln\left[1-e^{\beta\omega_{M,p_\mp}}\right] + e^{\beta(p_0-\mu)}\ln\left|\left(e^{\beta(\omega_{M,p_\mp}+p_0-\mu)}+1\right)\right|\right]
$$

$$
\left.+ \text{Li}_2\left(e^{\beta\omega_{M,p_\mp}}\right) + e^{\beta(p_0-\mu)}\text{Li}_2\left(-e^{\beta(\omega_{M,p_\mp}+p_0-\mu)}\right)\right\}. \tag{6.19}
$$

Also here, the sign cases correspond to a modified (d2).

Note that in the final expression for the purely thermal contribution, Eqs. (6.16)-(6.19), the mass parameters m_1, M should be replaced by $\min\{m_1, M\}$ and $\max\{m_1, M\}$ respectively; cf. Sec. 3.1.3.

The $(++)$-component of the self-energy of the fermionic eye-diagram presented in the above Sec. 6.1.1-6.1.3 has not been found in the literature.

6.1.4 Pseudoscalar emission off the fermion line

Analogously to Sec. 5, the pseudoscalar interaction with $\bar{\psi}^1\gamma_5\psi^2$ provides an additional vertex factor of γ_5 compared to the case of *scalar* emission considered in the previous three sections. In the naïve dimensional regularisation scheme, γ_5 anticommutes with the γ-matrix in the numerator of the fermion propagator and thereby provides an overall sign change together with a sign change of the numerator mass m_1. These sign changes are stated relative to the obtained results of Secs. 6.1.1-6.1.3 and a conclusion completely analogous to Sec. 5 is reached.

6.1.5 Scalar emission rate of the process $\psi^2 \to \psi^1\Phi$

The thermal rate for the scalar emission provided in this section is given by Eq. (2.125) in Sec. 2.7.2. In order to extract a probability observable from the self-energy presented in Secs. 6.1.1-6.1.3, that carries spin structure, it is advisable according to Weldon, (2.23) [13] to define

$$
\Sigma(p) = \bar{u}(p)i\mathcal{I}_{\text{bubble}}^{(++)}(p; m_1, M)u(p). \tag{6.20}
$$

This is the bubble contracted with incoming and outgoing states. These states satisfy the Dirac equation $(\not{p}-m)u(p) = 0$ as well as $\bar{u}(p)u(p) = 2\sqrt{p^2}$. In terms of Σ, the discontinuity over the real axis of this new scalar function may be related to the thermal decay rate. More specifically, the contraction of the three different pre-factors that appear in the self-energy and which contain explicit γ-matrices, is of interest. Assuming the external ψ^2 to be on-shell

$(p^2 = m_2^2)$, the contraction results in

$$\bar{u}(p)\left(\not{p}\left(1 + \tfrac{m_1^2 - M^2}{p^2}\right) + 2m_1 \right)u(p) = 2\left[p^2 + m_1^2 + 2m_1\sqrt{p^2} - M^2\right]$$

$$= -2M^2\left(1 - \frac{(m_1 + m_2)^2}{M^2}\right), \qquad (6.21)$$

$$\bar{u}(p)\left(\not{p} + \gamma^3 \frac{-p^2 + m_1^2 - M^2}{2|\mathbf{p}|} + m_1 \right)u(p) = p^2 + m_1^2 + 2m_1\sqrt{p^2} - M^2$$

$$= -M^2\left(1 - \frac{(m_1 + m_2)^2}{M^2}\right), \qquad (6.22)$$

$$\bar{u}(p)\left(-\gamma^0 + \gamma^3 \frac{p_0}{|\mathbf{p}|} \right)u(p) \equiv 0. \qquad (6.23)$$

The ratio of Eq. (2.127) may be obtained in the mass region of $m_2^2 \geq (m_1 + M)^2$ when putting the external ψ^2 on-shell ($p^2 = m_2^2$). The plotted ratio can be seen in Fig. 10 for a non-relativistic, slightly relativistic and highly relativistic incoming particle ψ^2. The figure is concerned with the limit $m_1 = M_\Phi = 0$, in which the ratio is not sensitive to m_1, M. In the limit $T \to 0$ the decay ratio $R_{\psi^2 \to \psi^1 \Phi} \to 1$.
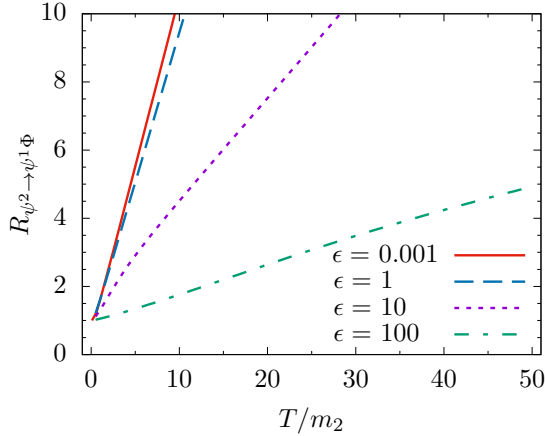

Figure 10: **Ratio to the zero-temperature limit of the emission rate of a scalar off a fermion line.** The ratio $R = \Gamma_D/\gamma_D$ is plotted for $m_2^2 \geq (m_1 + M_\Phi)^2$, below which the zero temperature quantity vanishes. Further, $m_1 = M_\Phi = 0$ is used as a simple case. Curves display ratios for varying $\epsilon = |\mathbf{p}|/m_2$ that parametrises the three-momentum for a non-relativistic $\epsilon \in \{0.001, 1, 10, 100\}$, slightly relativistic $\epsilon = 0.001$ and highly relativistic $\epsilon = 100$ incoming particle ψ^2.

The linear dependence of the self-energy on T seen in Fig. 10 is initially surprising in comparison to the quadratic dependence of the self-energy of the scalar-scalar loop seen Fig. 6. This difference in behaviour may be argued for [31] in the high-temperature limit. Then, the dependence on temperature of the free propagator comes from the term proportional to the thermal distribution function $n(|k_0|)$, see Eq. (2.95). Expanding this function at high temperatures (small β) results in different powers of T of the leading term for bosons and fermions respectively. For bosons, the temperature-dependence of the propagator is proportional to T while the leading term for the fermion propagator is constant in T. Hence, it is seen that for $T \to \infty$, the scalar-scalar loop of Sec. 3 contains a term that is quadratic in T (the purely thermal part) while the scalar-fermion loop of Sec. 6 contains terms proportional only to T.

7 Summary and conclusions

Thermal effects on observables have caught the interest of theoretical physicists over the last 50-60 years. Results are scattered in the literature and this thesis work presents a collection of decay rates for a theory containing generic (pseudo)scalar bosons and fermions. Several one-loop calculations were performed within the scope of this thesis using a very general formulation of thermal quantum field theory presented by Wagner [15]. Components of the self-energy were related to a quantity interpreted as the thermal decay rate of a field in an equilibrated medium. A (pseudo)scalar decaying into a (pseudo)scalar pair was considered as well as a (pseudo)scalar decaying into a fermion-antifermion pair. The rate of a (pseudo)scalar emission off a fermion line is also provided. For all these processes, except for the (pseudo)scalar decay to a fermion-antifermion pair, an enhancement of the thermal decay rate was found relative to the corresponding zero-temperature decay rate. In the case of a (pseudo)scalar decaying into two distinct (pseudo)scalars, this enhancement is quadratically growing with temperature, see Fig. 6a-c. Considering instead a scalar emission off a fermion line, the T-dependence is linear for high temperatures, see Fig. 10.

An interesting suppression is present in the case of a fermion-antifermion final state from an incoming (pseudo)scalar. The rate of this process was shown to be 0.25 times the zero-temperature quantity at high temperatures. From private communications with J. Bijnens [32], and by studying the imaginary-time analysis by Weldon [13], it is clear that the real-time self-energy is proportional to one factor of $(1 - n_{\mathrm{F}/\bar{\mathrm{F}}})$ for each outgoing fermion/antifermion. According to Weldon, this statement remains valid in the imaginary-time formalism for an n-particle final state and it is therefore expected to hold when more than two particles appear in the final state also in the real-time formalism. Hence, the outgoing particles are accompanied by Pauli suppression through the distribution function n_{F}; at high temperatures, this distribution approaches $1/2$ and the outgoing particles are Pauli blocked by medium particles with this probability. This fundamental effect is manifested in Fig. 7.

The one-loop self-energy for (anti)commuting fields had previously been written down in the imaginary-time formalism by Weldon [13]. Ho and Scherrer [28] extracted decay rates for the processes of Secs. 3-4 using the results of Weldon. This thesis confirms the thermal decay rate of [28] in the referenced sections within the real-time formalism. The decay rates have been further extended beyond the results of [28] to include chemical potentials, and, more importantly, the loop masses have been allowed to take on different values. Hence, a new momentum region $0 \leq p^2 < (m_1 - m_2)^2$ has been investigated for a (pseudo)scalar decaying into two (pseudo)scalars, a region in which decays are kinematically forbidden in zero-temperature theory.

The explicit real-time self-energy of the scalar-scalar loop has been published in [23] and was reproduced in this work. The equivalent quantity for the fermion loop has not been found in literature, although, for anticommuting fields, it appears in [13] in the imaginary-time formalism. However, the loop was presented there without the effects of spinor structure which has been incorporated in this thesis. The calculated decay rate of Fig. 7 reproduces the imaginary-time result of [28] if the loop-masses are taken to be identical.

The explicit real-time self-energy of the scalar-fermion loop has not been found in literature. Formally, the thermal decay rate is extracted from this self-energy, see Fig. 10. It is presented here as a hypothetical decay process not present within the framework of the Standard Model. Nevertheless, the thermal decay rate is presented in order to contribute to a complete understanding of the observables of thermal quantum field theory.

Lastly, the decay rate for a pseudoscalar transitioning into a pair of pseudoscalars, see Sec. 3, provides a provoking thought in relation to the baryon asymmetry problem. Through discussions with Antonio Rodríguez-Sánchez [33], the thought of important thermal effects on kaon-decays was lifted. The Standard Model provides the decay channels $K^0 \to \pi^0 \pi^0$ and $\bar{K}^0 \to \pi^0 \pi^0$, all of which are pseudoscalars. From the results of Fig. 6a-c, it may be expected that, after a careful analysis of those decays out of equilibrium, thermal effects could enhance both decay channels at high temperatures. If the amplitude of the two processes are different, thermal enhancement could provide a mechanism for significant CP violation. The violation of CP-symmetry is essential for the production of matter and antimatter at different rates according to the Sakharov conditions and hence necessary for explaining the observed lack of antimatter. It is therefore conceivable that a careful thermal treatment of the neutral kaon decay might shed light on the so far unexplained baryon asymmetry of the Universe. However, it is imperative to analyse the possibility to fulfil the remaining conditions of baryon number violation as well as out-of-equilibrium interactions.

Acknowledgements

References

[1] M. E. Peskin and D. V. Schroeder. *An introduction to quantum field theory*. Westview Press, 1995.

[2] R. P. Feynman and A. R. Hibbs. *Quantum mechanics and path integrals*. McGraw-Hill, 1965.

[3] P. T. Matthews and A. Salam. Propagators of quantized field. *Il Nuovo Cimento*, 2(1):120–134, July 1955.

[4] F. Bloch. Zur Theorie des Austauschproblems und der Remanenzerscheinung der Ferromagnetika. *Zeit. Phys.*, 74(5-6):295–335, May 1932.

[5] T. Matsubara. A new approach to quantum-statistical mechanics. *Prog. Theo. Phys.*, 14(4):351–378, October 1955.

[6] R. Kubo. Statistical-mechanical theory of irreversible processes. I. *J. Phys. Soc. Jpn.*, 12(6):570–586, June 1957.

[7] P. C. Martin and J. Schwinger. Theory of many-particle systems. I. *Phys. Rev.*, 115(6):1342–1373, September 1959.

[8] L. V. Keldysh. Diagram technique for nonequilibrium processes. *JETP*, 20(4):1018–1026, April 1965.

[9] H. Matsumoto, Y. Nakano, H. Umezawa, F. Mancini, and M. Marinaro. Thermo field dynamics in interaction representation. *Prog. Theo. Phys.*, 70(2):599–602, August 1983.

[10] A. J. Niemi and G. W. Semenoff. Finite-temperature quantum field theory in Minkowski space. *Ann. Phys.*, 152(1):105–129, January 1984.

[11] R. L. Kobes and K. L. Kowalski. Path-integral formulation of real-time finite-temperature field theory. *Phys. Rev. D*, 34(2):513–518, August 1986.

[12] N. P. Landsman and C. G. van Weert. Real- and imaginary-time field theory at finite temperature and density. *Phys. Rep.*, 145(3-4):141–249, January 1987.

[13] H. A. Weldon. Simple rules for discontinuities in finite-temperature field theory. *Phys. Rev. D*, 28(8):2007–2015, October 1983.

[14] P. Danielewicz. Quantum theory of nonequilibrium processes, I. *Ann. Phys.*, 152(2):239–304, February 1984.

[15] M. Wagner. Expansions of nonequilibrium Green's functions. *Phys. Rev. B*, 44(12):6104–6117, September 1991.

[16] M. Garny and M. M. Müller. Kadanoff-Baym equations with non-Gaussian initial conditions: the equilibrium limit. *Phys. Rev. D*, 80(8):085011, October 2009.

[17] L. Dolan and R. Jackiw. Symmetry behavior at finite temperature. *Phys. Rev. D*, 9(12):3320–3341, June 1974.

[18] H. A. Weldon. Chemical potentials in real-time thermal field theory. *Phys. Rev. D*, 76(12):125029, December 2007.

[19] A. S. Wightman. The general theory of invariant wave equations. In G. Velo and A. S. Wightman, editors, *Invariant wave equations*, volume 73, pages 24–59, Erice, June-July 1978. International school of mathematical physics held in Erice, Springer, Berlin, Heidelberg.

[20] N. P. Landsman. Consistent real-time propagators for any spin, mass, temperature and density. *Phys. Let. B*, 172(1):46–48, May 1986.

[21] J. Schwinger. Brownian motion of a quantum oscillator. *J. Math. Phys.*, 4(1):407–432, May-June 1961.

[22] H. Matsumoto, Y. Nakano, and H. Umezawa. An equivalence class of quantum field theories at finite temperature. *J. Math. Phys.*, 25(10):3076–3085, June 1984.

[23] T. Nishikawa, O. Morimatsu, and Y. Hidaka. Thermal sunset diagram for scalar field theories. *Phys. Rev. D*, 68(7):076002, January 2003.

[24] R. V. Kadison and J. R. Ringrose. *Fundamentals of the theory of operator algebra, I*, volume 1. Academic Press, Inc., 111 Fifth Avenue, New York, New York 10003, 1983.

[25] H. Umezawa, H. Matsumoto, and M. Tachiki. *Thermo field dynamics and condensed states.* North-Holland Publishing Company, 1982.

[26] A. Das. *Finite temperature field theory.* World Scientific Publishing Co. Pte. Ltd., 1997.

[27] Y. Fujimoto, M. Morikawa, and M. Sasaki. Imaginary part in thermo field dynamics. *Phys. Rev. D*, 33(2):590–593, January 1986.

[28] C. M. Ho and R. J. Scherrer. Cosmological particle decays at finite temperature. *Phys. Rev. D*, 92(2):025019, July 2015.

[29] J. A. Minahan. 8.323: QFT1 lecture notes. Lecture notes in QFT, MIT, 2011.

[30] A. J. Buras. Weak Hamiltonian, CP violation and rare decays. In *Probing the standard model of particle interactions. Proceedings, summer school in theoretical physics, NATO Advanced Study Institute, 68th session, Les Houches, France, July 28-September 5, 1997. Pt. 1, 2*, volume 1, pages 281–539, Les Houches, June 1998. NATO Advanced Study Institute, Elsevier Science B.V.

[31] R. Pasechnik. Priv. comm., 2020.

[32] J. Bijnens. Priv. comm., October 2019.

[33] A. Rodríguez-Sánchez. Priv. comm., 2019.